THE JOURNAL OF Pathology
The Journal of The Pathological Society
Understanding Disease

Anti-stromal treatment together with chemotherapy targets multiple signalling pathways in pancreatic adenocarcinoma.

Journal:	*The Journal of Pathology*
Manuscript ID	15-656.R1
Wiley - Manuscript type:	Original Research Article
Date Submitted by the Author:	n/a
Complete List of Authors:	Carapuça, Elisabete; Barts Cancer Institute, Tumour Biology Gemenetzidis, Emilios; Barts Cancer Institute, Tumour Biology Feig, Christine; Cancer Research Uk -Cambridge Research Institute-Li Ka Shing Centre, Genetic sequence and regulatory variation Bapiro, Tashinga; Cancer Research Uk -Cambridge Research Institute-Li Ka Shing Centre, Pharmacology & Drug Development Williams, Michael; Cancer Research Uk -Cambridge Research Institute-Li Ka Shing Centre, PK Analytics Core Facility Wilson, Abigail; Barts Cancer Institute, Tumour Biology Delvecchio, Francesca; Barts Cancer Institute, Tumour Biology Arumugam, Prabhu; Barts Cancer Institute, Tumour Biology Grose, Richard; Barts and The London, Tumour Biology Lemoine, Nicholas; Barts Cancer Institute, Molecular Oncology Richards, Frances; Cancer Research Uk -Cambridge Research Institute-Li Ka Shing Centre, Pharmacology & Drug Development Kocher, Hemant; Barts and the London, Barts Cancer Instititute
Tissue:	
Pathology:	
Technique:	

Anti-stromal treatment together with chemotherapy targets multiple signalling pathways in pancreatic adenocarcinoma.

Elisabete F. Carapuça[1#], Emilios Gemenetzidis[1#], Christine Feig[2], Tashinga E. Bapiro[2], Michael D. Williams[2], Abigail S. Wilson[1], Francesca R. Delvecchio[1], Prabhu Arumugam[1], Richard P. Grose[1], Nicholas R. Lemoine[3], Frances M. Richards[2], Hemant M Kocher[1,4*]

[1]Centres for Tumour Biology and [3]Molecular Oncology, Barts Cancer Institute – a CRUK Centre of Excellence, Queen Mary University of London, London EC1M 6BQ, UK.

[2]The University of Cambridge Cancer Research-UK Cambridge Institute, Li Ka Shing Centre, Robinson Way Cambridge, CB2 0RE, England.

[4]Barts and the London HPB Centre, The Royal London Hospital, Barts Health NHS Trust, London, E1 1BB, UK.

Running head: stroma and cancer co-targeting

***Corresponding author:** Hemant M Kocher MS MD FRCS, Queen Mary University of London, Centre for Tumour Biology, Barts Cancer Institute and CR-UK Clinical Centre, Barts & The London School of Medicine & Dentistry, Charterhouse Square, London EC1M 6BQ. UK.

Tel: +44(0) 20 7882 3579 Fax: +44(0) 20 7882 3884

Email: h.kocher@qmul.ac.uk

Disclosures: All authors have nothing to disclose.

#Contributed equally

Key words: Gemcitabine, all-trans-retinoic acid, quiescence, pancreatic stellate cells, collagen, fibronectin.

Total word count: 3187 Abstract word count: 260

Figures: 6 Supplementary Figures: 14 References: 40

Grant Support:

This work was supported by project grants from the Knowledge Transfer Network (Engineering and Physical Sciences Research Committee) and Pancreatic Cancer Research Fund (UK) to HMK. CF was supported by an EMBO long term fellowship and by a Marie Curie Intra-European Fellowship within the 7th European Community Framework Programme. TB and FR were supported by Cancer Research UK (grant C14303/A17197). Other grant funding includes project grants from Pancreatic Cancer Research Fund, Cancer Research UK and Barts Charity.

Acknowledgements:

This manuscript is dedicated to both parents of EFC, who sadly died during the study period. We thank members of the Kocher laboratory (Centre for Tumour Biology) for criticism and suggestions throughout this project. We thank Professor Ian Hart for comments on the manuscript. We thank Professor David A Tuveson (Cambridge Research Institute and Cold Spring Harbor Laboratory) for his critical insight and provision of KPC mice.

Author contributions:

Study concept, design and supervision and obtained funding: HMK; acquisition of data: EFC, EG, CF, MDW, TEB, ASW, FRD, PA, HMK; statistical analysis: EFC, HMK; drafting of the manuscript: HMK, EFC; technical or material support: RPG, FMR, NRL, HMK; analysis and interpretation of data as well as critical revision of the manuscript for important intellectual content: all authors.

Abbreviations:

ATRA: All-Trans Retinoic Acid;

BMP: bone morphogenetic protein;

FBS: Fetal Bovine Serum;

FGF: fibroblast growth factor;

FGFR: fibroblast growth factor receptor;

KPC: *LSL-Kras*$^{G12D/+}$*; LSL-Trp53*$^{R172H/+;}$ *Pdx-1-Cre*;

LC-MS: Liquid chromatography–mass spectrometry;

PDAC: Pancreatic Ductal Adenocarcinoma;

PSC: Pancreatic Stellate Cells;

RA: Retinoic Acid;

RARβ: Retinoic acid Receptor β;

SHH: sonic hedgehog;

STR: Short tandem repeat;

TGFβ: transforming growth factor β;

Abstract

Background & Aims: Stromal targeting for pancreatic ductal adenocarcinoma (PDAC) is rapidly becoming an attractive option, due to lack of efficacy of standard chemotherapy and increased knowledge about PDAC stroma. We postulated that combining stromal therapy may enhance anti-tumour efficacy of chemotherapy.

Methods: Gemcitabine and all-*trans* retinoic acid (ATRA) were combined in a clinically applicable regimen, to target cancer cells and pancreatic stellate cells (PSC) respectively, in 3D organotypic culture models and genetically engineered mice (*LSL-Kras*$^{G12D/+}$*;LSL-Trp53*$^{R172H/+}$*;Pdx-1-Cre* mice: KPC mice) representing the spectrum of PDAC.

Results: In two distinct sets of organotypic models as well as KPC mice, we demonstrate a reduction in cancer cell proliferation and invasion together with enhanced cancer cell apoptosis when ATRA is combined with Gemcitabine compared to vehicle or either agent alone. Simultaneously, PSC activity (in the form of deposition of extra-cellular matrix proteins such as Collagen and Fibronectin), and PSC invasive ability were both diminished in response to combination therapy. These actions were mediated by affecting a range of signalling cascades (Wnt, hedgehog, retinoid and FGF were studied) in cancer as well as stellate cells, effecting myriad epithelial cellular functions such as epithelial-mesenchymal transition, cellular polarity and lumen formation. At the tissue level, this resulted in enhanced tumour necrosis, increased vascularity, and diminished hypoxia. Consequently, there was an overall reduction in tumour size.

Conclusions: Stromal co-targeting (ATRA) alongside chemotherapy (Gemcitabine) is a potential clinical strategy. Experimental evidence suggests that the effect of this combination is mediated by dampening multiple signalling cascades in the tumour-stroma cross-talk, rather than ablating stroma or targeting a single pathway.

Introduction

Combination chemotherapy regimens consisting of oxaliplatin, irinotecan, fluorouracil, and leucovorin (FOLFIRINOX) [1] or nab-Paclitaxel with Gemcitabine [2] have resulted in increased median overall survival compared to Gemcitabine alone, which is the currently approved and widely used palliative mono-therapy [3]. However, gains have been marginal, and this may well be because desmoplasia remains largely unaltered with therapy[4].

PDAC is characterised by a pronounced desmoplastic stroma mediated by the activation of quiescent pancreatic stellate cells (PSC) [5]. This stroma creates a uniquely hypoxic microenvironment that, paradoxically, promotes both tumour growth and metastatic spread while inducing vascular collapse, thus creating a barrier to the perfusion/diffusion of therapeutic agents[6]; which, altogether, makes this cellular desmoplastic stroma an appealing therapeutic target. The pharmacologic inhibition of the sonic hedgehog signalling pathway in combination with Gemcitabine, in a genetically engineered mouse model, *LSL-Kras$^{G12D/+}$;LSL-Trp53$^{R172H/+}$;Pdx-1-Cre* (KPC) mice, produced variable results dependent on disease stage [7, 8], yet demonstrated proof-of-concept that stromal targeting was feasible. However, stromal ablation leads to a biologically more aggressive form of PDAC [8, 9], indicating that attention to the spatio-temporal aspects[4] of the tumour-stroma cross-talk is critical for its effective targeting [10].

PSC play a central role in desmoplastic stroma[11, 12]. Previously, we demonstrated that restoring the quiescent state of PSC, by replenishing their physiological retinol depots using the pleiotropic agent: all-trans retinoic acid (ATRA), halted tumour progression through targeting multiple dynamic tumour-stromal signalling cascades [13, 14]; a notion recently supported by targeting Vitamin D receptor [15]. In this report, we used combination therapy to target pancreatic cancer cells and their supporting stroma in *in vitro* and *in vivo* PDAC models to demonstrate efficacy of this strategy. It is feasible to target and normalize multiple altered signalling cascades mediating tumour-stroma cross-talk with this approach.

Methods

Organotypic cultures:

Short tandem repeat (STR) profiled cancer (Capan1, AsPC1) and stellate (PS1) cells were cultured, and pancreatic organotypic cultures were constructed as described elsewhere [11, 16-18]. Two cancer cell lines were utilised in organotypic models representing a spectrum of PDAC differentiation[11, 13, 18]. The pancreatic stellate cell line used was PS1, which was obtained from an unused normal pancreas (rejected for transplantation) donated by the UK human tissue bank (Ethics approval; Trent MREC (/MRE04/)). The cells were isolated in the laboratory, using the outgrowth method [19, 20] followed by immortalisation by expression of ectopic human telomerase reverse transcriptase (hTERT) [21], and verified as being of stellate cell origin by positive immunostaining for Desmin, Vimentin, αSMA and GFAP and ability to store Vitamin A [13].

In contrast to previous reports [13, 17], we allowed the cancer-stellate interaction to be established for 10 days [11], before commencing therapeutic dosing, for the treatment of an established tumour analogue. The cancer cell: stellate cell ratio was 1:2, as determined previously, providing the most aggressive, invasive phenotype within this model which mimicked histological features of advanced human cancer [11]. Multiple biological and technical replicates performed by two independent researchers ensured reproducibility. Treatment was given for two cycles, as per the human clinical protocol [3, 22],. Briefly, treatment of organotypic cultures was performed daily with ATRA (Sigma R2625, St. Louis, MO, USA) at 1μM or with weekly Gemcitabine (2', 2'-difluoro 2'-deoxycytidine, dFdC) (Eli Lilly, Indianapolis, IN, USA) at 100 nM (Capan-1/PS1) or 400 nM (AsPC1/PS1), or with the combination of Gemcitabine/ATRA or with respective vehicles. Organotypic cultures were harvested on day 24, fixed in 10% neutral buffered formalin (Cell Pathology BAF-001003A, Newton, UK), embedded in paraffin and cut into 4 μm sections. Each experiment had three technical replicates and at least three biologic repeats.

KPC mice treatment

All animal work was done in accordance with the UK Animals (Scientific Procedures) Act 1986, revised by the Amendment Regulations 2012 (SI 2012/3039) to transpose European Directive 2010/63/EU with approval from the local Animal Welfare and Ethical Review Body, and following the 2010 guidelines from the United Kingdom Coordinating Committee on Cancer Research [23]. Compound mutant KPC mice with mature, established tumours were enrolled at a median age of 180 days and used as described previously [7, 13]. ATRA was dissolved to 25mg/ml in dimethyl sulfoxide, further diluted to 2.98mg/ml in (2-Hydroxypropyl)-β-cyclodextrin (Sigma-Aldrich H5784) and finally to 1.5mg/ml with sterile filtered tap water. This ATRA solution was administered orally to mice at 15 mg/kg daily for seven days [13]. Gemcitabine was injected intraperitoneally at 100 mg/kg on days zero, three and seven [7]. The volume of the tumours was measured by ultrasound two days before the beginning of the treatment, and mice bearing tumour volume of ~250 mm^3 (Supplementary Table 1) were selected for the study. Tumours were harvested seven days after beginning of the treatment, and immediately submerged in formalin for 24 hours, followed by embedding in paraffin blocks for further sectioning and immunostaining analysis. The primary endpoint of study was drug efficacy as measured by a number of surrogate markers. Survival was not an endpoint analysis. Samples of tumours and serum were also snap-frozen for analysis of drug concentrations using LC-MS/MS.

Immunostaining

Paraffin-embedded sections were dewaxed and re-hydrated, and antigens were retrieved and immunostained for a range of markers to study cellular attributes using a range of antibodies (Supplementary Table 2) as described before [13, 16].

Quantification

The quantification of all cell counts and intensity of staining in the organotypic sections was performed on four-six representative pictures per organotypic gel of which there were three technical replicates for each of the biological repeats (minimum three). For the KPC mice, either the total tumour area or at least ten representative pictures per total tumour area were scanned using either Axioplan microscope (Zeiss 40 V 4.8.10, Carl Zeiss MicroImaging LLC, New York, US), confocal laser scanning microscope LSM 510 (Carl Zeiss MicroImaging LLC, New York, US) or Pannoramic 250 High Throughput Scanner (3DHISTECH Ltd., Budapest, Hungary). The intensities of fluorescence in the green/red channels were normalised with IgG controls and background fluorescence and calculated in an unbiased, blinded manner using either Adobe Photoshop CS6 (San Jose, CA USA), or Pannoramic Viewer Software (3DHISTECH Ltd., Budapest, Hungary), and Image J software (NIH, Maryland USA) as described before [13]. The methods for measurement of gel length and thickness, cancer and stellate total cell number per gel are described elsewhere [11].

Tissue Gemcitabine and ATRA levels

Tissue samples were homogenized in 50% acetonitrile:water at a concentration of 100 mg/mL using a precellys homogenizer. An aliquot of the homogenate was precipitated with acetonitrile containing a stable isotope (5 deuterium) label internal standard of ATRA. Measurement was carried out against a calibration line prepared in mouse plasma homogenate (100 mg/mL) in 50% acetonitrile:water. The MS/MS used was a Sciex 4000Qtrap equipped with a heated nebulizer atmospheric pressure chemical ionization source operating in the negative mode at 350ºC. MRM transitions were 301-205 and 306-205 for unlabelled and labelled ATRA respectively. LC was performed using a Dionex Ultimate 3000 LC and autosampler, using a gradient separation on a Phenomenex Kinetex 2.6 µm, 150x2.1 mm column. The binary gradient was run at 0.2 ml/min, starting at 40:60 A:B changing to 10:90 A:B from 0-15mins then holding from 15-17.6 minutes before quickly ramping back to 40:60 A:B at 17.62 minutes. The LC-MS/MS system was controlled by

Analyst 1.4 software. In order to ensure the correct isomer (ATRA) was measured a system suitability test was run at the beginning and end of the sample analysis to demonstrate separation of the ATRA isomer from the 9- and 13-cis isomers of retinoic acid (data not shown).

Fresh frozen tumour and plasma samples were processed and analysed for Gemcitabine and its metabolites by LC-MS/MS as previously described [24]. Briefly, LC-MS/MS was performed on a TSQ Vantage triple stage quadrupole mass spectrometer (Thermo Scientific, USA) fitted with a heated electrospray ionization (HESI-II) probe operated in positive and negative mode at a spray voltage of 2.5 KV, capillary temperature of 150ºC. Quantitative data acquisition was done using LC Quan2.5.6 (Thermo Fisher Scientific, USA).

Statistical analysis

Statistical analysis and graphical data representation were performed using the software PRISM V.6 (Graphpad, La Jolla, USA). Summary data are expressed as the median with interquartile range since the distribution was non-Gaussian. Comparisons were performed using Kruskal-Wallis test with Dunn's multiple comparison test. The level of significance was set at $P < 0.05$.

Results

Dosing schedule and timing for treatment of organotypic cultures and KPC mice with Gemcitabine and ATRA were designed to mimic clinically relevant treatment regimens for advanced human pancreatic cancer based on previously available data [3, 7, 11, 13, 22]. *In vitro* optimisations such as growth inhibition to 50% of control (GI_{50}) levels for Gemcitabine were determined for translation into the organotypic 3D model. Interestingly, we found the presence of extra-cellular matrix (ECM) protein in 3D model to have preferential cytoprotective effect on the pancreatic stellate cells (PSC). This resulted in different GI_{50} for both PSC and cancer cells in 3D models compared to 2D culture (Supplementary Figures 1, data not shown). Previously we had demonstrated ATRA had no direct effect on cancer cells by performing PSC or cancer cell alone organotypic cultures [13].

We then sought to identify effects on the cancer cells and stellate cells separately within this experimental design mimicking advanced PDAC. There was no change in gel contractility in organotypic cultures with any of the agents as compared to vehicle treatment (Supplementary Figure 2).

There was a significant reduction in proliferation of cancer cells induced by the presence of ATRA either alone or in combination with Gemcitabine *in vivo* as well as *in vitro*, across all experimental conditions (Figures 1A-C, Supplementary Figures 3A and B).No significant difference was noted for stellate cells proliferation after any of the treatments (Supplementary Figure 3C). However, induction of apoptosis was more pronounced with introduction of ATRA in the combination arm, suggesting that Gemcitabine potentiates the effect of ATRA (Figures 1D-F, Supplementary Figure 3D and E). We did not find any significant difference in the apoptotic index of stellate cells after any of the treatments, in both PDAC models (Supplementary Figure 3F). Cancer cell invasion into the extra-cellular matrix, a surrogate marker for metastatic capability, was also reduced by the combination treatment (Figures 2A-B, Supplementary Figure 4A-B).

PSC invasion into the ECM, and stellate cell density in mouse tumours, were reduced by ATRA treatment alone, and in combination with Gemcitabine (Figures 2C-E,

Supplementary Figures 4A-C). PSC numbers within organotypic gels did not change, reflecting the protective effect of matrix proteins on PSC in 3D, not seen in 2D *in vitro* state (Supplementary Figures 1B and 2D-E). However, the PSC activation state was altered by ATRA and the combination of Gemcitabine and ATRA, as indicated by a significant reduction in deposition of extra-cellular matrix (ECM) substrates such as Fibronectin and Collagen I, implying stromal re-modelling (Figures 3A-D, Supplementary Figures 5A-C).

Together with stromal re-modelling, we demonstrated increased vascularity of the KPC tumours, associated with decreasing hypoxia (Figures 3E, 3F, Supplementary Figures 6A, 6B). Surprisingly, despite this reduction in hypoxia, there was increased necrosis, *in vivo*, with combination treatment (Figure 4A, Supplementary Figure 6C). This resulted in smaller tumours in mice treated with combination therapy (Figure 4B). Certainly, with this regimen, both agents can be delivered successfully *in vivo* into the tumour parenchyma as measured by LC-MS/MS (Figures 4C-E). Furthermore, the tissue ATRA (not 9-cis and 13-cis RA) is directly correlated to serum ATRA measurements allowing surrogate measurements to be easily and readily performed (Figure 4C).

The precise mechanism(s) underpinning the success of this combination therapy are difficult to pinpoint, since ATRA influences multiple signalling cascades [13]. The enhanced apoptosis and reduction in proliferation of cancer cells may result from the reduction of Wnt signalling in the tumour compartment [13], disrupted fibroblast growth factor (FGF) signalling in the stromal compartment [17], or targeting of other signalling cascades such as Hedgehog, IL6, and CXCL12 amongst others [14].

In our experimental models, we could demonstrate a reduction in nuclear translocation of FGF2 and FGFR1 in PSC upon treatment of KPC mice and organotypic cultures with ATRA (Figures 5A-F, Supplementary Figures 7,8); this co-translocation being pertinent to PSC activity as demonstrated before [13]. There was enhanced nuclear Retinoic Acid Receptor β (RARβ) visibility within the PSC in KPC tumours upon treatment with ATRA (Figure 5G, Supplementary Figure 9A), which is known to reflect PSC quiescence [13]. Upregulation of PSC RARβ activity enhances secretion of secreted Frizzled related protein 4

(sFRP4) from the quiescent PSC as demonstrated before [13]. We could demonstrate increased stromal sFRP4 upon treatment with ATRA (Figure 5H, Supplementary Figure 9B). This modulation within PSC upon treatment with ATRA, in turn, led to reduced nuclear β-catenin, which translocates to the nucleus following canonical Wnt signalling activation [13, 25] (Figure 6A, Supplementary Figure 10). sFRP4 can sequester Wnt ligands within stroma to abrogate canonical Wnt signalling flux, and also act as gatekeeper, and, thus, affect epithelial-mesenchymal transition (EMT), apoptosis and invasion within cancer cells [26, 27].

In addition, there was reduction in Ezrin expression (Figure 6B, Supplementary Figure 11), which has previously been shown to enhance podosomal rosette formation [25]. Ezrin is also a marker for lumen formation and apico-basal polarity and such changes could be observed in the organotypic cultures more clearly than KPC mice but were difficult to quantify (data not shown). Furthermore, there was suppression in the expression of EMT activating transcription factors, as evidenced by reduction of nuclear *Twist1* and *Zeb1* in PDAC cells (Figures 6C and D, Supplementary Figures 12, 13), which may be related to reduction of canonical Wnt signalling [28]. Lastly, there was also reduction of nuclear and cytoplasmic Gli1 in cancer cells, suggesting reduced Hedgehog signalling in cancer cells [29] (Figure 6E, Supplementary Figure 14). The alteration of the vascular and immune sub-compartments of stroma, as shown by us before[14, 30], could also lead to enhanced necrosis in tumours *in vivo*, especially with combination treatment, ultimately resulting in tumour shrinkage.

Discussion

The effective reduced growth of the tumour size with a combination of stromal and cancer cell co-targeting is clinically relevant, since many locally advanced and borderline resectable cancers may be rendered surgically resectable using this regimen, a hypothesis which is now ready to be tested in clinical trials. The findings reported here are in sharp contrast to two recent studies exploring more radical approaches involving complete stromal ablation [8, 9] suggesting that stromal "normalisation" is much preferable over stromal ablation approaches [10]. Rhim et al, recently demonstrated that ablating sonic hedgehog-dependent stroma resulted in a more vascular tumour with poor differentiation, which, in part, could be abrogated by VEGF signalling blockade [8]. In a parallel approach, Ozdemir et al, by genetically ablating alpha-SMA-positive stroma, demonstrated presence of more invasive tumours, characterized with hypoxia, an epithelial-to-mesenchymal transition and alterations in immune surveillance. Specifically, this resulted in increased $CD4^{+}Foxp3^{+}$ T-regulatory cell infiltration, leading to a more aggressive tumour phenotype [8, 9]. In contrast, our findings suggest that restoring homeostatic stromal characteristics, rather than stromal ablation, have tumour-suppressive rather than a tumour-enhancing effect. This may be, in part, due to the homeostatic role of naturally occurring vitamin A analogue, and, in part, due to the pleiotropic actions of ATRA which are of relevance to pancreatic embryology and development.

Indeed, it has been demonstrated that ATRA influences multiple signalling cascades through selective retinoid receptor signalling (retinoid versus rexinoid receptors and isoforms of both subsets such as α,β,γ) in embryonic pancreas development, injury and regeneration [13, 31-34]. In particular, ATRA has a predominant effect on acinar morphology rather than endocrine cells, due to the epithelial-mesenchymal interactions in the developing pancreas [34]. Retinoic acid is critical for the developing pancreas, where it can interact with, and influence Wnt, TGFβ (transforming growth factor β), BMP (bone morphogenetic protein), and other signalling cascades [35], all of which are understood to be hijacked and altered by cancer cells to recruit stromal cells [36]. Previously we had demonstrated that restoring the

quiescent nature of PSC using ATRA can alter the signalling flux within the tumour-stroma [13] as well as intra-stromal cross-talk [14] of key pathways relevant to pancreatic cancer progression.

The enhanced apoptosis and reduction in proliferation of cancer cells, seen in this report, may result from reduction of canonical Wnt signalling in the tumour compartment, as a result of modification in the stromal compartment, by sequestering Wnt ligands, due to sFRP4 secretion [13]. Furthermore the disrupted fibroblast growth factor (FGF) signalling in the stromal compartment [17], or targeting of other signalling cascades such as Hedgehog, IL6, CXCL12 amongst others [14], could detrimentally effect the cancer cells by altering the signalling flux of, rather than selectively ablating, key cascades. FGF2/FGFR1 nuclear translocation is vital to activation of PSC which is required for cancer progression, as recently shown by us [17]. Other modifications in extra-cellular matrix deposition and re-modelling such as Collagen and Fibronectin can affect the cyto-protective micro-environment of cancer cells [37], internalisation and re-cycling of key integrins [18] and migration/invasion of cancer cells [38] as well as immune cells [14].

This alteration of a number of signalling pathways, in turn, may affect key epithelial cellular processes such apico-basal polarity [25], matrix re-modelling [18], epithelial-mesenchymal transition [26] and, thus, halt cancer progression. Therefore, multiple tumour-stroma cross-talk signalling cascades affecting numerous cancer and stellate cell processes are altered by ATRA when administered in clinically achievable dosing schedule.

Moreover, the alteration of immune cell infiltrate, vascularity and hypoxia demonstrated by us previously [13, 14, 30] in relation to stromal targeting therapy is relevant to this combination treatment. We demonstrate, here, that chemotherapy is more effective when combined with ATRA in altering intra-stromal or peri-tumoural cross-talk in the tissue micro-environment, particularly the enhancement of vascularity and the consequent reduction in hypoxia. In fact, it has been long understood that the tumour micro-environment exerts a protective influence on the cancer cells through multiple mechanisms such as resistance to alkylating agents [39], direct cell-cell contact between cancer and stromal cells [40],

through many signalling cascades, thus enhancing the tumour cell autonomous resistance to chemotherapy. We were unable to detect enhanced levels of active metabolite of Gemcitabine, and we speculate this may be related to increased necrotic component of the tumour which will not contain active metabolite. In addition, the consistency of the results obtained from these two different PDAC models (one *in vitro*, one *in vivo*) suggests that the organotypic models may be useful preclinical tools for dissection of the molecular signalling pathways involved in PDAC drug resistance. Modulating the 3D OT cultures would recapture important aspects of the tumour microenvironment that can influence cancer cell behaviour.

Thus, based on data presented here, we postulate that the effect of this combination strategy of co-targeting cancer and stromal cells is more likely to involve dampening of a multitude of signalling cascades, rather than via a single, specific pathway or mechanism and, therefore, altering a number of key cellular processes. This notion concurs with separate attempts to restore homeostatic capability of desmoplastic stroma by targeting the vitamin D receptor [15], as well as normalisation of vascularisation with dual-action combination therapy [30]. Given the known fat-soluble vitamin deficiency in patients with PDAC, due to biliary and pancreatic duct obstruction, the proposal to restore homeostatic stromal function, in conjunction with cancer targeting with conventional chemotherapy, appears to be a viable therapeutic opportunity underpinned by the clinical features of this cancer. This hypothesis, thus, has enough rationale to be explored in a human clinical trial involving patients with PDAC.

References

1. Conroy T, Desseigne F, Ychou M, et al. FOLFIRINOX versus gemcitabine for metastatic pancreatic cancer. N Engl J Med 2011;364:1817-25.
2. Von Hoff DD, Ervin T, Arena FP, et al. Increased survival in pancreatic cancer with nab-paclitaxel plus gemcitabine. N Engl J Med 2013;369:1691-703.
3. The use of gemcitabine for the treatment of pancreatic cancer (TA25). National Institute for Health and Clinical Excellence. 2001.
4. Neesse A, Algul H, Tuveson DA, et al. Stromal biology and therapy in pancreatic cancer: a changing paradigm. Gut 2015;64:1476-84.
5. Neesse A, Michl P, Frese KK, et al. Stromal biology and therapy in pancreatic cancer. Gut 2011;60:861-8.
6. Provenzano PP, Cuevas C, Chang AE, et al. Enzymatic targeting of the stroma ablates physical barriers to treatment of pancreatic ductal adenocarcinoma. Cancer Cell 2012;21:418-29.
7. Olive KP, Jacobetz MA, Davidson CJ, et al. Inhibition of Hedgehog signaling enhances delivery of chemotherapy in a mouse model of pancreatic cancer. Science 2009;324:1457-61.
8. Rhim AD, Oberstein PE, Thomas DH, et al. Stromal elements act to restrain, rather than support, pancreatic ductal adenocarcinoma. Cancer Cell 2014;25:735-47.
9. Ozdemir BC, Pentcheva-Hoang T, Carstens JL, et al. Depletion of carcinoma-associated fibroblasts and fibrosis induces immunosuppression and accelerates pancreas cancer with reduced survival. Cancer Cell 2014;25:719-34.
10. Froeling FE, Kocher HM. Homeostatic restoration of desmoplastic stroma rather than its ablation slows pancreatic cancer progression. Gastroenterology 2015;148:849-50.
11. Kadaba R, Birke H, Wang J, et al. Imbalance of desmoplastic stromal cell numbers drives aggressive cancer processes. J Pathol 2013;230:107-17.
12. Apte MV, Wilson JS, Lugea A, et al. A starring role for stellate cells in the pancreatic cancer microenvironment. Gastroenterology 2013;144:1210-9.
13. Froeling FE, Feig C, Chelala C, et al. Retinoic Acid-Induced Pancreatic Stellate Cell Quiescence Reduces Paracrine Wnt-beta-Catenin Signaling to Slow Tumor Progression. Gastroenterology 2011;141:1486-97.
14. Ene-Obong A, Clear AJ, Watt J, et al. Activated pancreatic stellate cells sequester CD8+ T cells to reduce their infiltration of the juxtatumoral compartment of pancreatic ductal adenocarcinoma. Gastroenterology 2013;145:1121-32.
15. Sherman MH, Yu RT, Engle DD, et al. Vitamin d receptor-mediated stromal reprogramming suppresses pancreatitis and enhances pancreatic cancer therapy. Cell 2014;159:80-93.
16. Coleman SJ, Watt J, Arumugam P, et al. Pancreatic cancer organotypics: High throughput, preclinical models for pharmacological agent evaluation. World J Gastroenterol 2014;20:8471-81.
17. Coleman SJ, Chioni AM, Ghallab M, et al. Nuclear translocation of FGFR1 and FGF2 in pancreatic stellate cells facilitates pancreatic cancer cell invasion. EMBO Mol Med 2014;6:467-81.
18. Li NF, Gemenetzidis E, Marshall FJ, et al. RhoC interacts with integrin alpha5beta1 and enhances its trafficking in migrating pancreatic carcinoma cells. PLoS One 2013;8:e81575.
19. Apte MV, Haber PS, Applegate TL, et al. Periacinar stellate shaped cells in rat pancreas: identification, isolation, and culture. Gut 1998;43:128-33.
20. Bachem MG, Schneider E, Gross H, et al. Identification, culture, and characterization of pancreatic stellate cells in rats and humans. Gastroenterology 1998;115:421-32.
21. Li NF, Kocher HM, Salako MA, et al. A novel function of colony-stimulating factor 1 receptor in hTERT immortalization of human epithelial cells. Oncogene 2009;28:773-80.

22. Burnett AK, Hills RK, Grimwade D, et al. Inclusion of chemotherapy in addition to anthracycline in the treatment of acute promyelocytic leukaemia does not improve outcomes: results of the MRC AML15 trial. Leukemia 2013;27:843-51.
23. Workman P, Aboagye EO, Balkwill F, et al. Guidelines for the welfare and use of animals in cancer research. Br J Cancer 2010;102:1555-77.
24. Bapiro TE, Frese KK, Courtin A, et al. Gemcitabine diphosphate choline is a major metabolite linked to the Kennedy pathway in pancreatic cancer models in vivo. Br J Cancer 2014;111:318-25.
25. Kocher HM, Sandle J, Mirza TA, et al. Ezrin interacts with cortactin to form podosomal rosettes in pancreatic cancer cells. Gut 2009;58:271-84.
26. Ford CE, Jary E, Ma SS, et al. The Wnt gatekeeper SFRP4 modulates EMT, cell migration and downstream Wnt signalling in serous ovarian cancer cells. PLoS One 2013;8:e54362.
27. Pohl S, Scott R, Arfuso F, et al. Secreted frizzled-related protein 4 and its implications in cancer and apoptosis. Tumour Biol 2015;36:143-52.
28. Garg M. Epithelial-mesenchymal transition - activating transcription factors - multifunctional regulators in cancer. World J Stem Cells 2013;5:188-95.
29. Briscoe J, Therond PP. The mechanisms of Hedgehog signalling and its roles in development and disease. Nat Rev Mol Cell Biol 2013;14:416-29.
30. Wong PP, Demircioglu F, Ghazaly E, et al. Dual-action combination therapy enhances angiogenesis while reducing tumor growth and spread. Cancer Cell 2015;27:123-37.
31. Colvin EK, Susanto JM, Kench JG, et al. Retinoid signaling in pancreatic cancer, injury and regeneration. PLoS One 2011;6:e29075.
32. Tulachan SS, Doi R, Kawaguchi Y, et al. All-trans retinoic acid induces differentiation of ducts and endocrine cells by mesenchymal/epithelial interactions in embryonic pancreas. Diabetes 2003;52:76-84.
33. Kobayashi H, Spilde TL, Bhatia AM, et al. Retinoid signaling controls mouse pancreatic exocrine lineage selection through epithelial-mesenchymal interactions. Gastroenterology 2002;123:1331-40.
34. Kadison A, Kim J, Maldonado T, et al. Retinoid signaling directs secondary lineage selection in pancreatic organogenesis. J Pediatr Surg 2001;36:1150-6.
35. Pearl EJ, Bilogan CK, Mukhi S, et al. Xenopus pancreas development. Dev Dyn 2009;238:1271-86.
36. Jones S, Zhang X, Parsons DW, et al. Core signaling pathways in human pancreatic cancers revealed by global genomic analyses. Science 2008;321:1801-6.
37. Mantoni TS, Lunardi S, Al-Assar O, et al. Pancreatic stellate cells radioprotect pancreatic cancer cells through beta1-integrin signaling. Cancer Res 2011;71:3453-8.
38. Lu J, Zhou S, Siech M, et al. Pancreatic stellate cells promote hapto-migration of cancer cells through collagen I-mediated signalling pathway. Br J Cancer 2014;110:409-20.
39. Teicher BA, Herman TS, Holden SA, et al. Tumor resistance to alkylating agents conferred by mechanisms operative only in vivo. Science 1990;247:1457-61.
40. Fujita H, Ohuchida K, Mizumoto K, et al. Tumor-stromal interactions with direct cell contacts enhance proliferation of human pancreatic carcinoma cells. Cancer Sci 2009;100:2309-17.

Figure Legends

Figure 1. Effect on cancer cells proliferation and apoptosis after combination treatment with Gemcitabine and ATRA.

Summary data from organotypic cultures (OT) and *LSL-Kras$^{G12D/+}$;LSL-Trp53$^{R172H/+}$;Pdx-1-Cre* mice (KPC mice) treated with either vehicle, Gemcitabine alone, ATRA alone or a combination of Gemcitabine with ATRA as shown by median and interquartile range as box and whisker (min-max) plots. All observations were normalized to controls (vehicle). 9-15 experimental replicates were carried out for OT resulting in 35-50 high power field measurements. 5-6 mice per group were enrolled to allow assessments in 10-30 high power fields. Comparisons were made by Kruskal-Wallis test followed by Dunn's post-hoc analysis. **** P<0.001, ** P< 0.01, * P<0.05*. PSC: Pancreatic stellate cell.

Cancer cell proliferation index in organotypics (A,B) and KPC mice (C).

Cancer cell apoptotic index in organotypics (D,E) and KPC mice (F).

Please see Supplementary Figure 3 for representative images.

Figure 2. Effect on cancer and stellate cells invasion after combination treatment with Gemcitabine and ATRA.

Summary data from organotypic cultures (OT) and *LSL-Kras$^{G12D/+}$;LSL-Trp53$^{R172H/+}$;Pdx-1-Cre* mice (KPC mice) treated with either vehicle, Gemcitabine alone, ATRA alone or a combination of Gemcitabine with ATRA as shown by median and interquartile range as box and whisker (min-max) plots. All observations were normalized to controls (vehicle). 9-15 experimental replicates were carried out for OT resulting in 35-50 high power field measurements. 5-6 mice per group were enrolled to allow assessments in 10 high power fields. Comparisons were made by Kruskal-Wallis test followed by Dunn's post-hoc analysis. **** P<0.001*, *** P<0.01*, ** P<0.05*. PCC: Pancreatic cancer cell; PSC: Pancreatic stellate cell.

Cancer cell invasion index in organotypics (A,B).

Stellate cell invasion index in an organotypic model (C, D)

Stellate cell density in KPC mice (E). Stellate cell density in KPC was determined as green signal pixel intensity per area; the number of stellate cells was not counted as it was not possible to identify accurately this cell type in the KPC tumour section.

Please see Supplementary Figure 4 for representative images.

Figure 3. Effect on pancreatic stellate cell activity, vascularity and hypoxia after combination treatment with Gemcitabine and ATRA.

Summary data from organotypic cultures (OT) and *LSL-Kras$^{G12D/+}$;LSL-Trp53$^{R172H/+}$;Pdx-1-Cre* mice (KPC mice) treated with either vehicle, Gemcitabine alone, ATRA alone or a combination of Gemcitabine with ATRA as shown by median and interquartile range as box and whisker (min-max) plots. All observations were normalized to controls (vehicle). 9-15 experimental replicates were carried out for organotypics resulting in 35-50 high power field measurements. 5-6 mice per group were enrolled to allow assessments in 10-30 high power fields. Comparisons were made by Kruskal-Wallis test followed by Dunn's post-hoc analysis. **** P<0.001, ** P< 0.01, * P<0.05*. PSC: Pancreatic stellate cell.

Stellate cell activity in terms of fibronectin deposition in an organotypic model (A,B) and KPC mice (C) and, in terms of Collagen I deposition in the KPC mouse model (D).

Vascular density as determined by Endomucin stain in the KPC mouse model (E). Hypoxic index as determined by GLUT-1 stain (F).

Please see Supplementary Figures 5 and 6 for representative images.

Figure 4. Effect of combination treatment with Gemcitabine and ATRA on tumour growth, Gemcitabine and ATRA intra-tumoural levels in KPC mice.

(A) Percentage necrotic area as determined by H&E slides. Summary data from *LSL-Kras$^{G12D/+}$;LSL-Trp53$^{R172H/+}$;Pdx-1-Cre* mice (KPC mice) treated with either vehicle,

Gemcitabine alone, ATRA alone or a combination of Gemcitabine with ATRA as shown by median and inter-quartile range as box and whisker (min-max) plots. 5-6 mice per group were enrolled. Comparisons were made by Kruskal-Wallis test followed by Dunn's post-hoc analysis. *** *P<.001, ** P< 0.01, * P<0.05*. See Supplementary Figure 6C for representative images.

(B) Percentage change in tumour volume between pre-treatment (Day -2) and post-treatment (Day 7) was measured by ultrasound in the KPC mice model.

(C) Serum and pancreatic tumour ATRA concentration demonstrated correlation in mice receiving ATRA treatment (Pearson's correlation coefficient 0.66 (95% CI 0.09-0.9)). A regression line and it's 95% confidence intervals are shown.

(D) ATRA tumour tissue concentration in KPC mice treated with ATRA or Gem/ATRA

(E) Tumour tissue gemcitabine metabolites in Gem and Gem/ATRA treated mice.

ns: not significant.

Figure 5: The combination of Gemcitabine with ATRA affects multiple embryonic signalling cascades in cancer cells and stroma in organotypic cultures and KPC mice. Summary data from organotypic cultures (OT) and *LSL-Kras$^{G12D/+}$;LSL-Trp53$^{R172H/+}$;Pdx-1-Cre* mice (KPC mice) treated with either vehicle, Gemcitabine alone, ATRA alone or a combination of Gemcitabine with ATRA as shown by median and interquartile range as box and whisker (min-max) plots. All observations were normalized to controls (vehicle). Sections from three experimental replicates were carried out for organotypics resulting in 18 high power field measurements. Three mice per group were selected to allow assessments in 10 high power fields per section. Comparisons were made by Kruskal-Wallis test followed by Dunn's post-hoc analysis. *** *P<0.001, * P<0.05*.

FGF2 nuclear expression index in organotypics and KPC mice (A-C).

FGFR1 nuclear expression index in organotypics and KPC mice (D-F).

RARβ nuclear expression index in KPC mice (G).

sFRP4 stromal expression index in KPC mice (H).

Please see supplementary figures 7, 8 and 9 for representative images.

Figure 6: The combination of Gemcitabine with ATRA affects apical polarity, epithelial-mesenchymal transition and hedgehog signalling in cancer cells within organotypic cultures and KPC mice.

Representative images from organotypic cultures (OT) and *LSL-Kras$^{G12D/+}$;LSL-Trp53$^{R172H/+}$;Pdx-1-Cre* mice (KPC mice), as indicated, treated with either vehicle, Gemcitabine alone, ATRA alone or the combination of Gemcitabine with ATRA. Bold arrowheads used to indicate positive stain and other arrowheads to indicate negative stain.

A) Capan-1 cells stained with an anti-cytokeratin antibody (green) and anti-β-catenin (red) antibody was used to localize the presence of β-catenin in organotypic cultures. Cytokeratin positive cancer cells demonstrate loss of nuclear β-catenin in ATRA treated organotypic cultures. Please see Supplementary Figure 10 for detailed data on KPC mice and organotypic cultures. Scale bar 10μm.

B) Anti-cytokeratin antibody (green) and anti-Ezrin antibody (red) were used to localize the presence of Ezrin in KPC mice. Cytokeratin positive cancer cells demonstrate loss of membranous Ezrin in ATRA treated murine tissues. Please see Supplementary Figure 11 for detailed data on KPC mice and organotypic cultures.

C) Anti-cytokeratin antibody (green) and anti-Twist1 (red) antibody were used to localize the presence of *Twist1* in Capan1/PS1 organotypic cultures. Cytokeratin-positive cancer cells demonstrate loss of nuclear *Twist1* in ATRA organotypic cultures. Cytokeratin negative PSC demonstrate nuclear *Twist1* to act as an internal positive control. Please see Supplementary Figure 12 for detailed data on KPC mice and organotypic cultures.

D) Anti-Zeb1 antibody (green) and anti-E-cadherin (red) antibody were used to localize the presence of *Zeb1* in Capan1/PS1 organotypic cultures. E-cadherin-positive cancer cells demonstrate loss of nuclear *Zeb1* in ATRA organotypic cultures. E-cadherin negative PSC

demonstrate nuclear *Zeb1* to act as an internal positive control. Please see Supplementary Figure 13 for detailed data on KPC mice and organotypic cultures.

E) In KPC mice, anti-Gli1 staining (brown) was used to localize Gli1 expression. Loss of Nuclear Gli1 in epithelial appearing cells was demonstrable within ATRA treated murine PDAC tissues. Please see Supplementary Figure 14 for detailed data on KPC mice.

Scale bar 10μm.

Figure 1

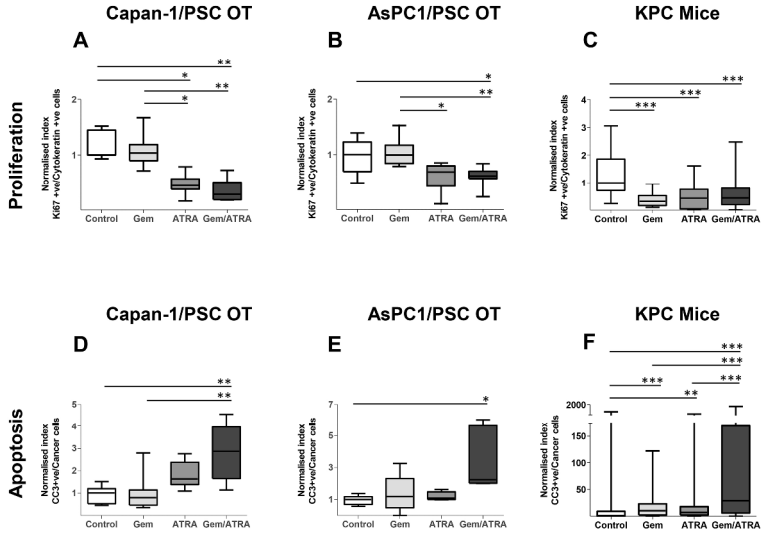

Effect on cancer cells proliferation and apoptosis after combination treatment with Gemcitabine and ATRA
275x397mm (300 x 300 DPI)

Figure 2

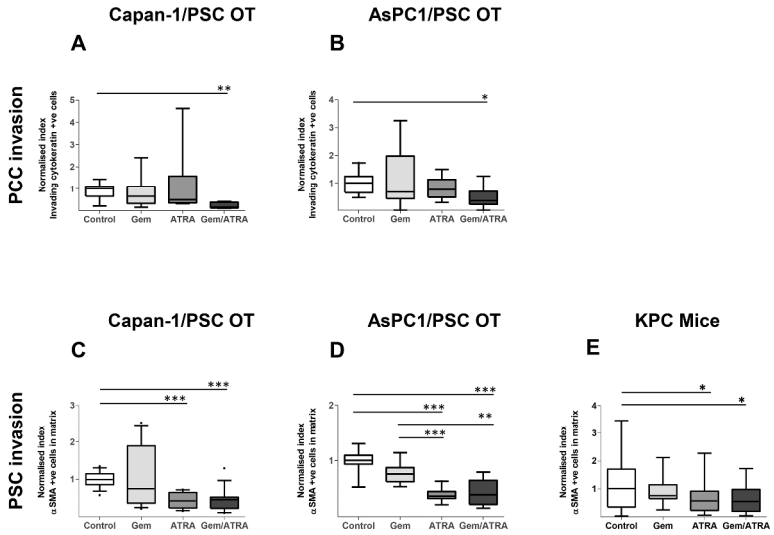

Effect on cancer and stellate cells invasion after combination treatment with Gemcitabine and ATRA
275x397mm (300 x 300 DPI)

Figure 3

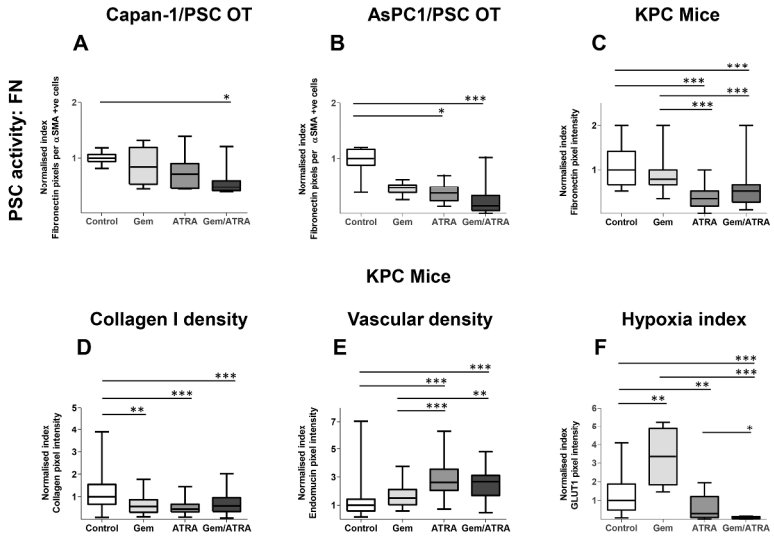

Effect on pancreatic stellate cell activity, vascularity and hypoxia after combination treatment with Gemcitabine and ATRA
275x397mm (300 x 300 DPI)

Figure 4

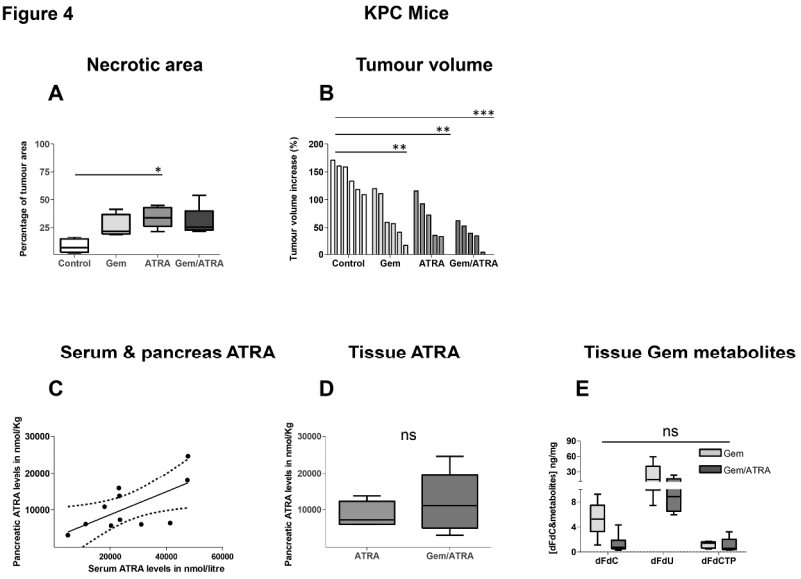

Effect of combination treatment with Gemcitabine and ATRA on tumour growth, Gemcitabine and ATRA intra-tumoural levels in KPC mice
275x397mm (300 x 300 DPI)

Figure 5

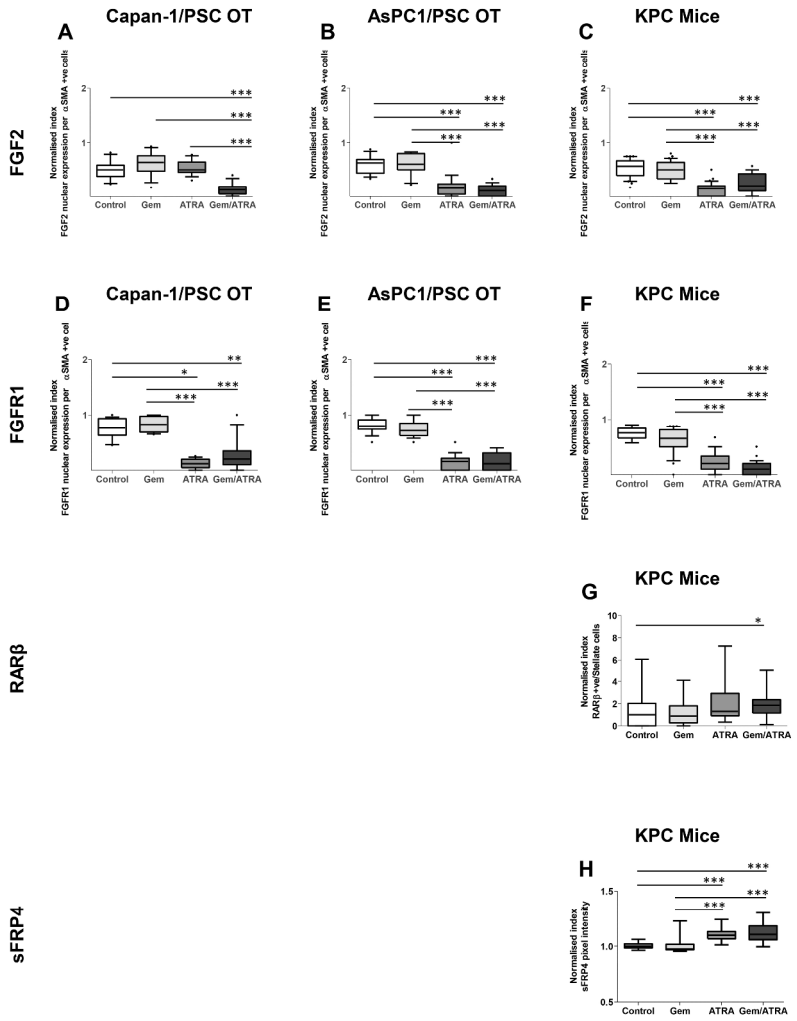

The combination of Gemcitabine with ATRA affects multiple embryonic signalling cascades in cancer cells and stroma in organotypic cultures and KPC mice
275x397mm (300 x 300 DPI)

Figure 6

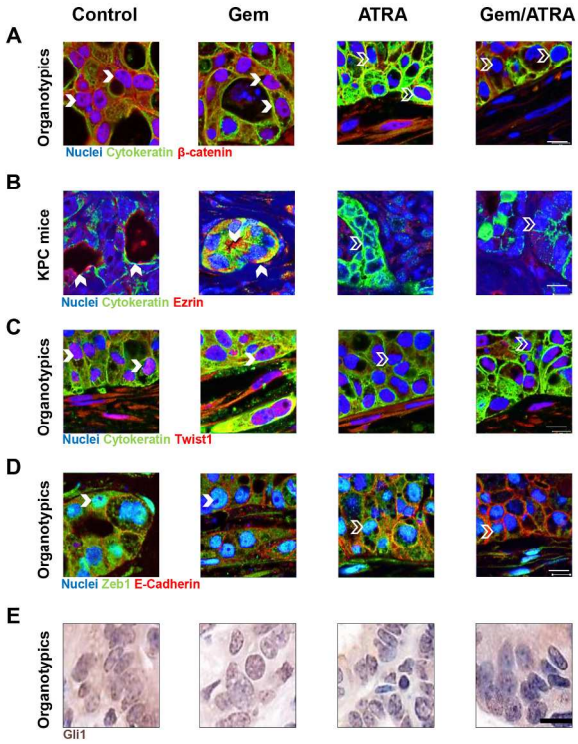

The combination of Gemcitabine with ATRA affects apical polarity, epithelial-mesenchymal transition and hedgehog signalling in cancer cells within organotypic cultures and KPC mice
190x275mm (300 x 300 DPI)

Anti-stromal treatment together with chemotherapy targets multiple signalling pathways in pancreatic adenocarcinoma.

Elisabete F. Carapuça[1#], Emilios Gemenetzidis[1#], Christine Feig[2], Tashinga E. Bapiro[2], Michael D. Williams[2], Abigail S. Wilson[1], Francesca R. Delvecchio[1], Prabhu Arumugam[1], Richard P. Grose[1], Nicholas R Lemoine[3], Frances M. Richards[2], Hemant M Kocher[1,4]*

[1]Centres for Tumour Biology and [3]Molecular Oncology, Barts Cancer Institute – a CRUK Centre of Excellence, Queen Mary University of London, London EC1M 6BQ, UK.

[2]The University of Cambridge Cancer Research-UK Cambridge Institute, Li Ka Shing Centre, Robinson Way Cambridge, CB2 0RE, England.

[4]Barts and the London HPB Centre, The Royal London Hospital, Barts Health NHS Trust, London, E1 1BB, UK.

Running title: stroma and cancer co-targeting

***Corresponding author:** Hemant M Kocher MS MD FRCS, Queen Mary University of London, Centre for Tumour Biology, Barts Cancer Institute – a CRUK Centre of Excellence, Charterhouse Square, London EC1M 6BQ, UK.

Tel: +44(0) 20 7882 3579; Email: h.kocher@qmul.ac.uk

#Contributed equally

Supplementary Figure 1: Design of experiments and determination of dosing schedule.

A) Determination of Gemcitabine GI_{50} (Cytotoxic effect: growth inhibition of 50%) alone, or in combination with ATRA (1μM), on AsPC1 (blue and black lines) or Capan1 (green and red lines) cell growth. Pancreatic cancer cell lines AsPC-1 and Capan1 in 2D monoculture were exposed once, to different concentrations of Gemcitabine, and were allowed to grow for a period of up to seven days, prior to assessing proliferation rates. The GI_{50} for Gemcitabine was determined as 240nM for AsPC1, and 48nM for Capan1, indicating that AsPC1 cells are more resistant to Gemcitabine, when compared to Capan1 cell line. Addition of daily ATRA, to this treatment regimen had no effect on the GI_{50} curves of either cell line, indicating the lack of any combinational effect of ATRA with Gemcitabine in 2D monocultures on cancer cells.

B) Determination of Gemcitabine GI_{50} alone or in combination with ATRA (1μM) on pancreatic stellate cells (PSC) growth. PSC showed sensitivity to Gemcitabine (GI_{50} 26nM), which increased when treatment was combined with daily ATRA exposure. At least, in 2D cultures, the actively proliferating PSC appear to be sensitive to Gemcitabine.

C) i) Treatment protocol of the 3D organotypic cultures with Gemcitabine weekly for two consecutive weeks, mimicking treatment currently in use in the clinic (1). Representative images of H&E stained sections of gels resultant from AsPC1 **(ii)** or Capan1 **(iii)** organotypic cultures, treated with Gemcitabine at various doses in order to determine Gemcitabine GI_{50} (concentration that reduces epithelial cell layer thickness by 50%). Gemcitabine GI_{50} was slightly higher at 300nM for AsPC1 and 100nM for Capan1 organotypic cultures than in the 2D monocultures. The increased value of GI_{50} is anticipated due to cyto-protective effect of organized 3D matrix particularly Collagen I (2). Intriguingly PSC layer thickness was unaffected by Gemcitabine treatment, when PSC and cancer cells were combined (data not shown).

D) Representative image of a section of an organotypic culture treated with BrdU (red) and stained with a cytokeratin antibody (green) to delineate cancer cells. Representative graph of the percentage of cancer and stellate cells with BrdU incorporation. To determine the rates of nucleoside uptake in organotypic cultures, BrdU pulse chase was carried out. BrdU is an analogue of the nucleoside thymidine, and Gemcitabine an analogue of cytidine. BrdU was administered at the same concentrations that Gemcitabine would be added to the 3D co-culture models. The percentage of incorporation of BrdU by PSC was much less than by tumour cells, which confirms that Gemcitabine has minimal cytotoxic effect on PSC in organotypic culture model. This effect may be due to a slower proliferation rate of PSC. Thus, they do not incorporate the nucleoside analogue at the same rate as cancer cells. Therefore, the cytotoxic effect of Gemcitabine is largely specific to the epithelial cancer cells.

Supplementary Figure 2: **The combination treatment of Gemcitabine with ATRA does not affect PSC number, and consequently gel length and thickness is also unchanged.**

A) Schematic representation of an organotypic culture of admixed cancer cells and PSC, seeded on top of gel composed of Matrigel and Collagen I that mimics the tumour ECM environment. Measurements of cancer cell layer thickness, gel length, gel thickness are schematically represented and have been previously described (3).

B, C) Cancer cell layer thickness was unaffected in presence of PSC in Capan1/PS1 (B) and AsPC1/PS1 (C) organotypic cultures, respectively, upon treatment with vehicle, Gemcitabine alone, ATRA alone or a combination of Gemcitabine and ATRA.

D,E) Total PSC number was also unaffected in Capan1/PS1 (D) and AsPC1/PS1 (E) organotypic cultures respectively upon treatment.

F,G) Gel thickness was also unaffected in Capan1/PS1 (F) and AsPC1/PS1 (G) organotypic cultures, respectively, upon treatment.

H,I) Gel length was also unaffected in Capan1/PS1 (H) and AsPC1/PS1 (I) organotypic cultures, respectively, upon treatment.

9-15 experimental replicates were carried out for organotypic cultures. Comparisons were made by Kruskal-Wallis test followed by Dunn's post-hoc analysis.

ns: not significant

Supplementary Figure 3: The combination of Gemcitabine with ATRA affects cancer cell proliferation, apoptosis in organotypic cultures, as well as in KPC mice.

A) Representative images from organotypic cultures (OT) treated with either vehicle, Gemcitabine alone, ATRA alone or the combination of Gemcitabine with ATRA. Capan1 cells stained with an anti-cytokeratin antibody (green) and proliferating Capan1 cells stained with an anti-Ki67 antibody (red) to determine ratio of proliferating cancer cells per field.

B) Representative images of tumour sections from *LSL-Kras$^{G12D/+}$;LSL-Trp53$^{R172H/+}$;Pdx-1-Cre* mice (KPC mice) treated with vehicle, Gemcitabine, ATRA or Gemcitabine with ATRA, and stained with an anti-CK8 antibody (red) and proliferating cancer cells stained with an anti-Ki67 antibody (green) to determine the ratio of proliferating cancer cells per field.

C) Representative images from organotypic cultures (OT) after same treatment regimen, where Stellate cells were stained with an anti-alpha-SMA antibody in green and with an anti-Ki67 antibody (red) to determine ratio of proliferating stellate cells per field.

D) Representative images of organotypic gel sections where Capan1 cells were stained by immuno-histochemistry with an anti-cleaved caspase-3 antibody. Apoptotic cancer cells were identified by the cytoplasmic brown staining. There was no staining within the PSC layer. Percentage apoptotic cancer cells (based on morphology) were determined.

E) Representative images of tumour sections from KPC mice stained with an anti-cleaved caspase-3 antibody to determine apoptotic cells. There was no staining in non-epithelial compartment. Percentage apoptotic cancer cells (based on morphology) were determined.

F) Representative images of tumour sections from KPC mice stained by immunofluorescence with an anti-alpha-SMA antibody and with an anti-cleaved caspase-3 antibody to determine the ratio of apoptotic stellate cells. There was no staining in the stromal compartment.

Supplementary Figure 4: The combination of Gemcitabine with ATRA affects cancer and stellate cell invasion in organotypic cultures as well as stellate cells density in KPC mice.

A) Representative images of organotypic gel sections where Capan1 cells were stained with a cytokeratin antibody (green) and PSC were stained with an anti-αSMA antibody (red) to identify the cells that have invaded the gel. The yellow line marks the junction between the PSC layer and the extracellular matrix (top of the gel). The number of invading cells was counted directly on the section on the Axioplan microscope, to accurately identify the top of the gel and identify the cell type and number that invaded into the gel.

B) i and ii) Representative H&E stained image from a Capan-1/PS1 OT section that clearly shows the cancer cell layer, the gel and the top of the gel where the stellate cell layer is demonstrable. The dashed black line in ii) marks the top of the gel. Invading cells were counted below the black line..

C) Representative images of tumour sections from KPC mice stained with an anti-αSMA antibody (green) to identify PSC. Stromal cell density was determined by green pixel intensity. Pericytes were accounted for as described in Figure 6A. Scale bar 100 μm (except C where Scale bar = 50 μm).

Supplementary Figure 5: ATRA alters stellate cells activation status.

A) Representative images of organotypic sections where Capan1 cells were stained with an anti-Cytokeratin antibody (green) and extra-cellular matrix (ECM) deposition by an anti-Fibronectin antibody (red). Note: the ECM gel formed at inception with Collagen I and Matrigel contains no fibronectin. Hence, fibronectin shown here represents ECM generated by cells co-cultured in 3D. Fibronectin deposition was only present around PSC, indicating PSC were source of this ECM protein. Fibronectin deposition was normalized to PSC number to determine PSC activity as shown in Supplementary Figure 2. Scale bar 100 µm.

B) Representative images of tumour sections from *LSL-Kras$^{G12D/+}$;LSL-Trp53$^{R172H/+}$;Pdx-1-Cre* mice (KPC mice) stained by immuno-histochemistry with anti-Fibronectin antibody. Fibronectin expression was scored based on intensity and degree of brown staining as described before (4). Scale bar 50 µm.

C) Representative images of Collagen deposition in KPC mice tumour sections stained with Picrosirius Red. Pixel intensity was determined as described before (5). Scale bar 100 µm.

Supplementary Figure 6: The combination treatment of Gemcitabine with ATRA alters the vascular density, hypoxic environment and the necrosis pattern in murine tumours.

A) Representative images of tumour sections from *LSL-Kras$^{G12D/+}$;LSL-Trp53$^{R172H/+}$;Pdx-1-Cre* mice (KPC mice) stained with an anti-Endomucin antibody (red) to identify blood vessels and an anti-αSMA antibody (green) to identify stellate cells as well as pericytes. The number of blood vessels increased in the tumour/stromal area of PDAC tumours of mice treated with ATRA or with the combination Gemcitabine /ATRA, while at the same time there is a reduction of αSMA expression (after subtracting doubly stained structures to exclude pericytes). Scale bar 100 μm.

B) Representative images KPC mice tumour sections stained with an anti-GLUT1 antibody (green) to mark hypoxic areas in the tumours. Pixel intensity determined level of hypoxia as described before (6). Scale bar 100 μm.

C) Representative images of H&E stained tumour sections from mice. Necrotic areas, identified by morphology, are marked by the dotted lines in black. Percentage of necrotic area was determined based on total surface area of tumour. Scale bar 5000 μm.

Supplementary Figure 7: ATRA treatment affects pancreatic stellate cell activity by reducing the nuclear translocation FGF2.

A-D) Representative images of sections from *LSL-Kras$^{G12D/+}$;LSL-Trp53$^{R172H/+}$;Pdx-1-Cre* mice (KPC mice) stained with an anti-FGF2 antibody (red) and an anti-Cytokeratin antibody (green) to identify epithelial cells.

E-H) Representative images of Capan1/PS1 organotypic (OT) sections stained with same antibodies as KPC mice. There is a clear reduction of nuclear FGF2 expression in stromal cells (Cytokeratin –ve cells) from mice treated with ATRA. Scale bar 50 μm.

a-d) Zoom in images of the marked areas of KPC main images (A-D) with bold arrowheads pointing to nuclear FGF2 expressing stromal cells and empty arrowheads pointing to stromal cells not expressing FGF2 in the nucleus.

e-h) Zoom in images of the marked areas of OT main images (E-H) also with bold and empty arrowheads pointing to the difference of nuclear FGF2 expression in stellate cells upon treatment with ATRA. Scale bar 10 μm.

Supplementary Figure 8: ATRA treatment affects the pancreatic stellate cell activity by reducing the nuclear translocation of FGFR1.

A-D) Representative images of sections from *LSL-Kras$^{G12D/+}$;LSL-Trp53$^{R172H/+}$;Pdx-1-Cre* mice (KPC mice) stained with an anti-FGFR1 antibody (red) and an anti-αSMA antibody (green) to identify stromal cells.

E-H) Representative images of Capan1/PS1 organotypic (OT) sections stained with same antibodies as KPC mice. There is a clear reduction of nuclear FGFR1 expression in stromal αSMA-positive cells in the mice treated with ATRA. Scale bar 50 μm.

a-d) Zoom in images of the marked areas of KPC main images (A-D) with bold arrowheads pointing to nuclear FGFR1 expressing stromal cells and empty arrowheads pointing to stromal cells with no nuclear FGFR1 expression.

e-h) Zoom in images of the marked areas of OT main images (E-H) also with bold and empty arrowheads pointing to the difference of nuclear FGFR1 expression in stellate cells upon treatment with ATRA which is in concordance with FGF2 expression pattern seen in Supplementary figure 8. Scale bar 10 μm.

Supplementary Figure 9: Nuclear RARβ expression in, and stromal sFRP4 secretion by, pancreatic stellate cells is altered upon treatment with ATRA alone and in combination with Gemcitabine.

A) Representative images of tumour sections from *LSL-Kras$^{G12D/+}$;LSL-Trp53$^{R172H/+}$;Pdx-1-Cre* mice (KPC mice) stained by immuno-histochemistry with an anti-RARβ antibody. Nuclear RARβ expression is most enhanced in stellate cells of sections from mice treated with ATRA. Zoom in images show the amplification of the marked areas of main images, which show the nuclear RARβ expression in stetalle cells of sections from ATRA treated mice in comparison to Vehicle or Gemcitabine alone treated mice. Scale bar 100 μm. Zoom in images: Scale bar 10 μm.

B) Representative images of tumour sections from KPC mice stained by immuno-histochemistry with an anti-sFRP4 antibody. Stromal sFRP4 expression is most enhanced in tumour surrounding environment of sections from mice treated with ATRA alone or in combination with Gemcitabine. Scale bar 50 μm. Zoom in images show a significant expression of sFRP4 in the stroma of tumour from ATRA or ATRA/Gemcitabine combination treated mice in comparison to Vehicle or Gemcitabine alone treated mice. Zoom in images: Scale bar 10 μm.

Supplementary Figure 10: ATRA disrupts Wnt-β-catenin signalling pathway.

A-D) Representative images of tumour sections from *LSL-Kras$^{G12D/+}$;LSL-Trp53$^{R172H/+}$;Pdx-1-Cre* mice (KPC mice) stained with an anti-β-catenin antibody (red) and an anti-Cytokeratin antibody (green) to identify epithelial cells.

E-H) Representative images of Capan1/PS1 organotypic (OT) sections stained with same antibodies as KPC mice sections. Scale bar 50 μm.

a-d) Zoom in images of the marked areas of KPC main images (A-D) with bold arrowheads pointing to nuclear β-catenin expression in epithelial cells and empty arrowheads pointing to no nuclear β-catenin expression.

e-h) Zoom in images of marked areas of OT main images (E-H) also with bold and empty arrowheads pointing to the differences of nuclear β-catenin expression in epithelial cells. There is a shift of the spatial β-catenin localization that spans from the cell nuclei, in epithelial cell either from KPC tumours or OT cultures treated with vehicle or Gemcitabine alone to the cell membrane upon treatment with ATRA or Gemcitabine and ATRA. Scale bar 10 μm.

Supplementary Figure 11: The combination treatment affects the lumen formation and apico-basal polarity of cancer cells.

A-D) Representative images of tumour sections from *LSL-Kras$^{G12D/+}$;LSL-Trp53$^{R172H/+}$;Pdx-1-Cre* mice (KPC mice) stained with an anti-Ezrin antibody (red) and an anti-Cytokeratin antibody (green) to identify epithelial cells.

E-H) Representative images of Capan1/PS1 organotypic (OT) sections stained with same antibodies as KPC mice sections. Scale bar 50 µm.

a-d) Zoom in images of the marked areas of KPC main images (A-D) with bold arrowheads pointing to Ezrin cell membrane expression in cancer cells and empty arrowheads pointing to loss of membranous Ezrin expression.

e-h) Zoom in images of the marked areas of OT main images (E-H) also with bold and empty arrowheads pointing to the differences in Ezrin expression in cancer cells. Ezrin expression is reduced in cancer cells of KPC mice tumours or OT cultures, after the combination treatment (Gemcitabine with ATRA). Scale bar 10 µm.

Supplementary Figure 12: ATRA alone or in combination with Gemcitabine nuclear *Twist*1 expression within cancer cells.

A-D) Representative images of tumour sections from *LSL-Kras*$^{G12D/+}$;*LSL-Trp53*$^{R172H/+}$;*Pdx-1-Cre* mice (KPC mice) stained with an anti-Twist1 antibody (red) and an anti-Cytokeratin antibody (green).

E-H) Representative images of Capan1/PS1 organotypic (OT) sections stained with same antibodies as KPC mice sections. Scale bar 50 μm.

a-d) Zoom in images of the marked areas of KPC main images (A-D) with bold arrowheads pointing to nuclear *Twist*1 expression in epithelial cells expression and empty arrowheads pointing to loss of this nuclear *Twist*1 expression.

e-h) Zoom in images of the marked areas of OT main images (E-H) also with bold and empty arrowheads pointing to the differences of nuclear *Twist*1 expression in epithelial cells upon different treatment conditions. ATRA alone or in combination with Gemcitabine reduces nuclear *Twist*1 expression in epithelial cells, whilst in stellate cells nuclear *Twist*1 expression remains unaltered. Scale bar 10 μm.

Supplementary Figure 13: The combination treatment affects the nuclear translocation of transcription factor *ZEB*1 in cancer cells.

A-D) Representative images of tumour sections from *LSL-Kras*$^{G12D/+}$*;LSL-Trp53*$^{R172H/+}$*;Pdx-1-Cre* mice (KPC mice) stained with an anti-Zeb1 antibody (red) and an anti-αSMA antibody (green).

E-H) Representative images of Capan1/PS1 organotypic (OT) sections stained with an anti-E-cadherin antibody (red) and an anti-Zeb1 antibody (green). Scale bar 50 μm.

a-d) Zoom in images of the marked areas of KPC main images (A-D) with bold arrowheads pointing to nuclear *Zeb1* expression within epithelial cells and empty arrowheads pointing to loss of nuclear *Zeb*1 expression.

e-h) Zoom in images of the marked areas of OT main images (E-H) also with bold and empty arrowheads pointing to the differences of nuclear *Zeb*1 expression in epithelial cells upon different treatment conditions. ATRA in combination with Gemcitabine reduces nuclear *Zeb*1 expression in epithelial cells, whilst in stellate cells nuclear *Zeb*1 expression remains unaltered. Scale bar 10 μm.

Supplementary Figure 14: The combination treatment affects the Hedgehog signalling in cancer cells.

A) Representative images of tumour sections from *LSL-Kras$^{G12D/+}$;LSL-Trp53$^{R172H/+}$;Pdx-1-Cre* mice (KPC mice) stained by immuno-histochemistry with an anti-Gli1 antibody. Zoom in images show the clear expression of nuclear and cytoplasmic Gli1 in ductal cells sections from untreated or Gemcitabine treated mice in comparison to a reduction of Gli1 expression in cancer cells of ATRA/Gemcitabine treated mice.

B) Representative images of OT sections stained by immuno-histochemistry with an anti-Gli1 antibody. Zoom in images clearly show the reduction in Gli expression of cancer cells from Gemcitabine/ATRA treated OT cultures, which is in agreement with the differences in Gli1 expression also observed in KPC mice. Scale bar 100 μm. Zoom in images: Scale bar 10 μm.

Supplementary table 1: KPC mice characteristics at recruitment

Treatment type	Age (days)	Tumour volume (mm^3 on 2 days before treatment as measured by ultrasound)
Control	249	137.761
Control	188	303.706
Control	170	326.367
Control	117	163.306
Control	120	195.04
Control	128	149.467
Gemcitabine	211	124.714
Gemcitabine	200	274.747
Gemcitabine	189	232.725
Gemcitabine	177	284.779
Gemcitabine	176	149.722
Gemcitabine	102	191.824
ATRA	216	156.138
ATRA	177	302.217
ATRA	243	327.712
ATRA	223	211.803
ATRA	150	160.042
ATRA + Gemcitabine	119	324.267
ATRA + Gemcitabine	171	234.933
ATRA + Gemcitabine	185	263.636
ATRA + Gemcitabine	218	495.181
ATRA + Gemcitabine	204	239.703
ATRA + Gemcitabine	124	343.271

Supplementary table 2: Table of antibodies

Sections species origin	Antibody	Catalogue reference	Incubation period	Antigen retrieval method	IF (or IHC) dilution
Organotypic sections (anti-human)	Rabbit Cytokeratin	DAKO Z0662	1h, RT	HIER	1:200
	Mouse Fibronectin	SIGMA F0916	ON, 4^0C	Pepsin	1:100
	Mouse Ki67	DAKO M7240	1h, RT	HIER	1:100
	Mouse αSMA	DAKO M0851	1h, RT	HIER	1:300
	Rabbit CC3	Cell signaling D175	1h, RT	HIER	1:400 (IHC)
	Rabbit Gli1*	Chemicon AB3444	1h, RT	HIER	1:300 (IHC)
	Mouse E-Cadherin	Abcam ab1416	ON, 4^0C	HIER	1:100
	Rabbit RAR-β*	Abcam ab53161	1h, RT	HIER	1:200 (IHC)
	Mouse Twist1*	Abcam ab50887	ON, 4^0C	HIER	1:100
	Rabbit Zeb1*	Santa cruz sc-25388	ON, 4^0C	HIER	1:500
	Mouse FGF2*	Millipore 05-118	ON, 4^0C	HIER	1:100
	Rabbit FGFR1*	Abcam ab10646	ON, 4^0C	HIER	1:500
	Rabbit SFRP4*	Santa cruz sc-30152	1h, RT	N.A.	1:50 (IHC)
	Mouse Ezrin*	BD 10603	ON, 4^0C	HIER	1:200
	Mouse β-Catenin*	BD 610154	ON, 4^0C	HIER	1:200
KPC mouse sections (anti-mouse)	Rabbit CK8	Abcam ab59400	ON, 4^0C or 1h, RT	HIER	1:100
	Rabbit Fibronectin	Abcam ab23750	1h, RT	HIER	1:200 (IHC)
	Rabbit Ki67	Abcam ab15580	1h, RT	HIER	1:150
	Mouse αSMA	SIGMA F3777	ON, 4^0C	HIER	1:500
	Rabbit CC3	Cell signaling	1h, RT	HIER	1:400 (IHC)

		D175			
	Rat Endomucin	Santa Cruz Sc-65495	1h, RT	HIER	1:100
	Rabbit Glut1	Millipore 07-1401	ON, 4^0C	HIER	1:250

ON: overnight; 1h: one hour, RT; room temperature;

HIER: Heat Induced Epitope Retrieval (citrate buffer pH6)

N.A.: not applicable

*: used also in mouse

References:

1. The use of gemcitabine for the treatment of pancreatic cancer (TA25). In: National Institute for Health and Clinical Excellence; 2001.
2. Dangi-Garimella S, Sahai V, Ebine K, Kumar K, Munshi HG. Three-dimensional collagen I promotes gemcitabine resistance in vitro in pancreatic cancer cells through HMGA2-dependent histone acetyltransferase expression. PLoS One 2013;8:e64566.
3. Kadaba R, Birke H, Wang J, Hooper S, Andl CD, Di Maggio F, Soylu E, et al. Imbalance of desmoplastic stromal cell numbers drives aggressive cancer processes. J Pathol 2013;230:107-117.
4. Ene-Obong A, Clear AJ, Watt J, Wang J, Fatah R, Riches JC, Marshall JF, et al. Activated pancreatic stellate cells sequester CD8+ T cells to reduce their infiltration of the juxtatumoral compartment of pancreatic ductal adenocarcinoma. Gastroenterology 2013;145:1121-1132.
5. Wong P-P, Demircioglu F, Ghazaly E, Alrawashdeh W, Stratford MR, Scudamore CL, Cereser B, et al. Dual-action combination therapy enhances angiogenesis while reducing tumor growth and spread. Cancer Cell 2015:In Press.
6. Wong PP, Demircioglu F, Ghazaly E, Alrawashdeh W, Stratford MR, Scudamore CL, Cereser B, et al. Dual-action combination therapy enhances angiogenesis while reducing tumor growth and spread. Cancer Cell 2015;27:123-137.

Supplementary Figure 1

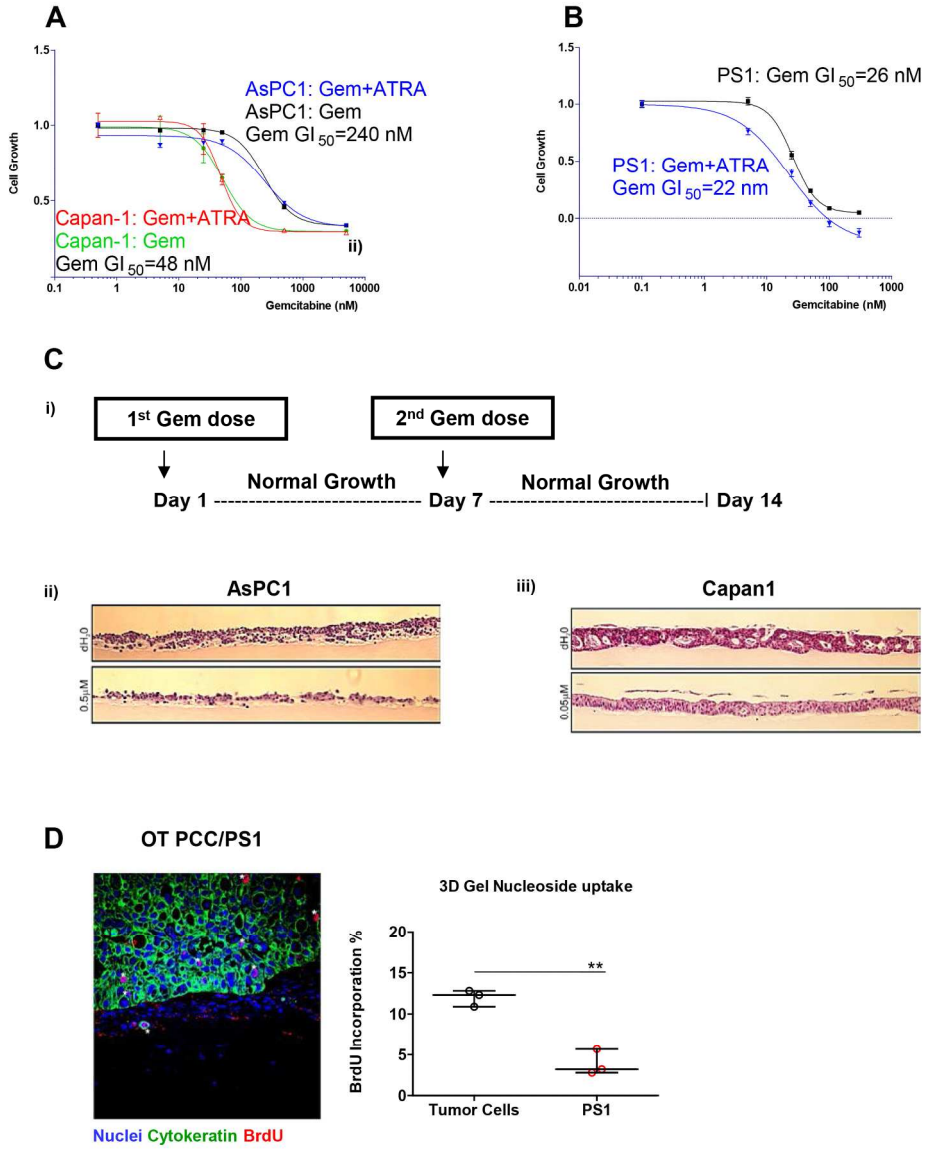

189x238mm (300 x 300 DPI)

Supplementary Figure 2

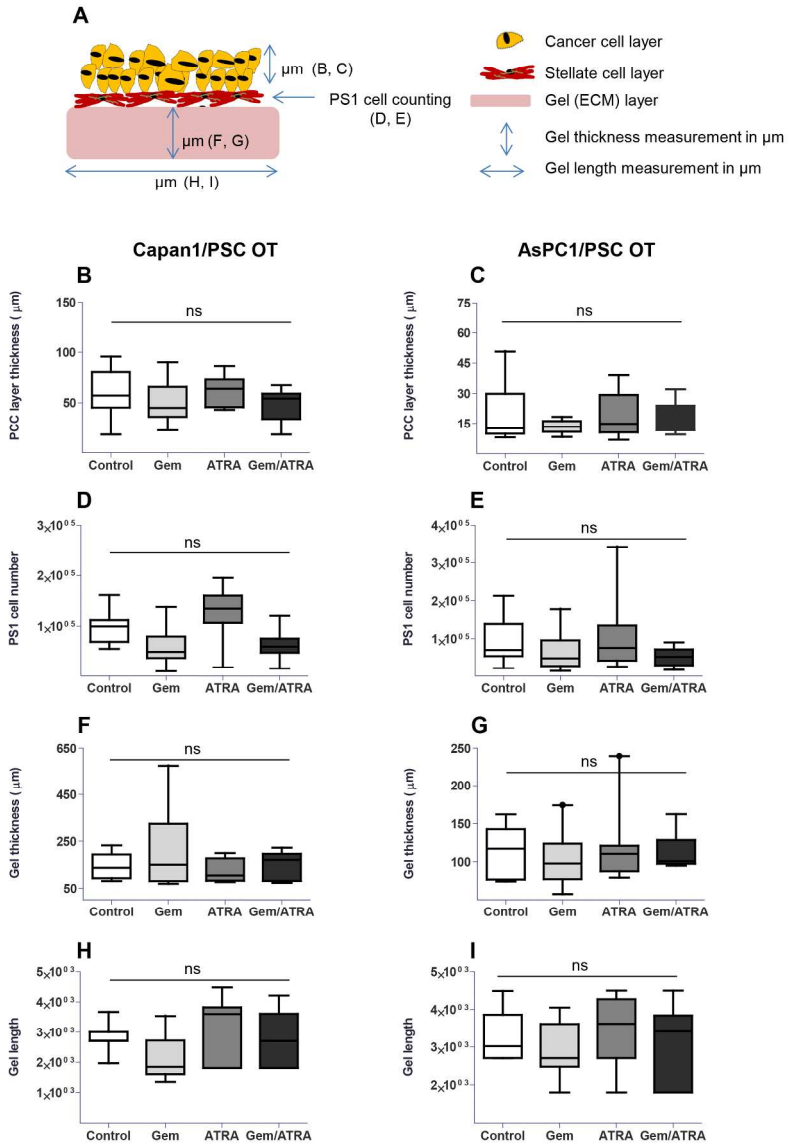

184x266mm (300 x 300 DPI)

Supplementary Figure 3

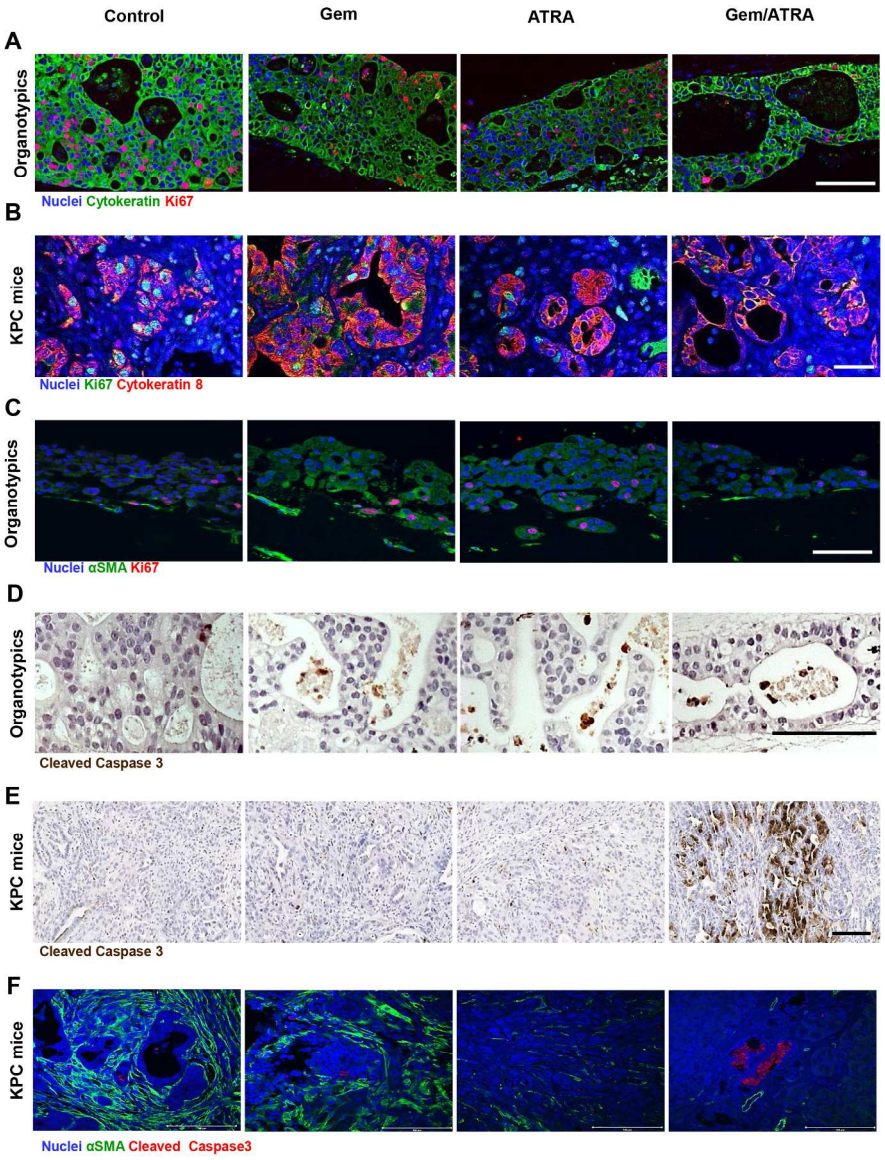

189x249mm (300 x 300 DPI)

Supplementary Figure 4

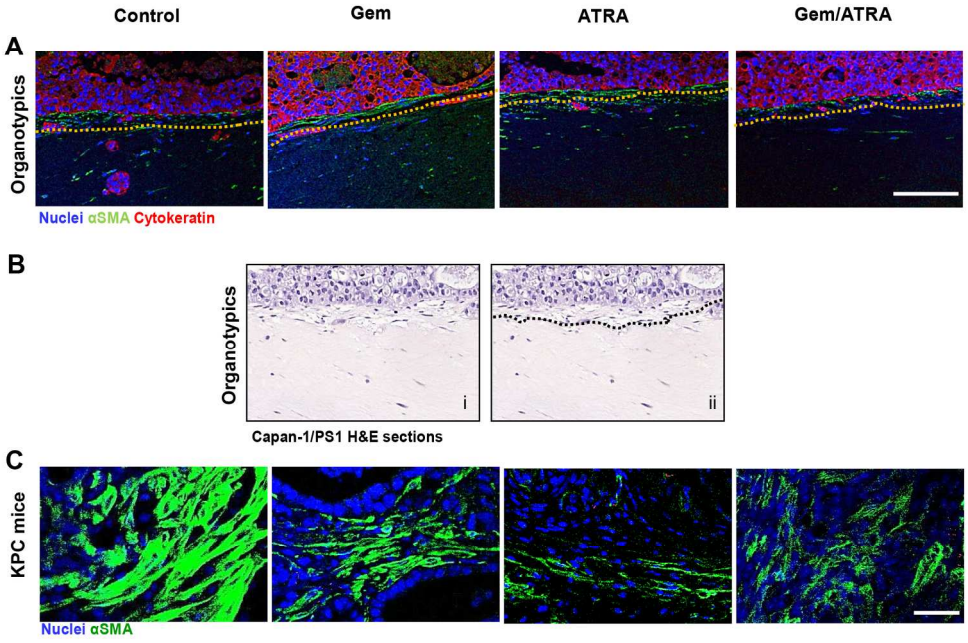

189x131mm (300 x 300 DPI)

Supplementary Figure 5

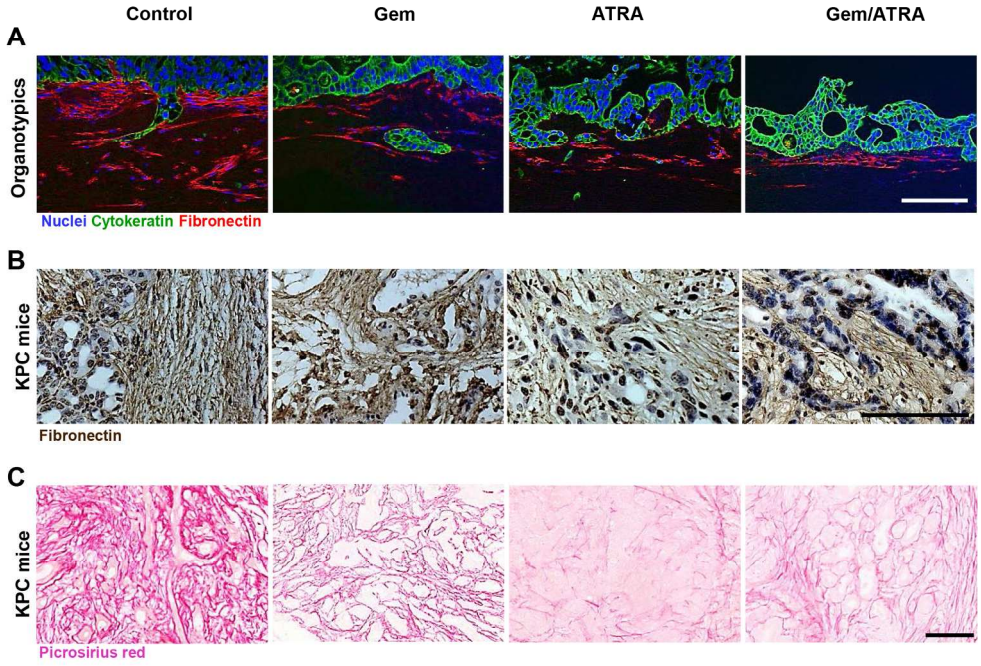

189x139mm (300 x 300 DPI)

Supplementary Figure 6

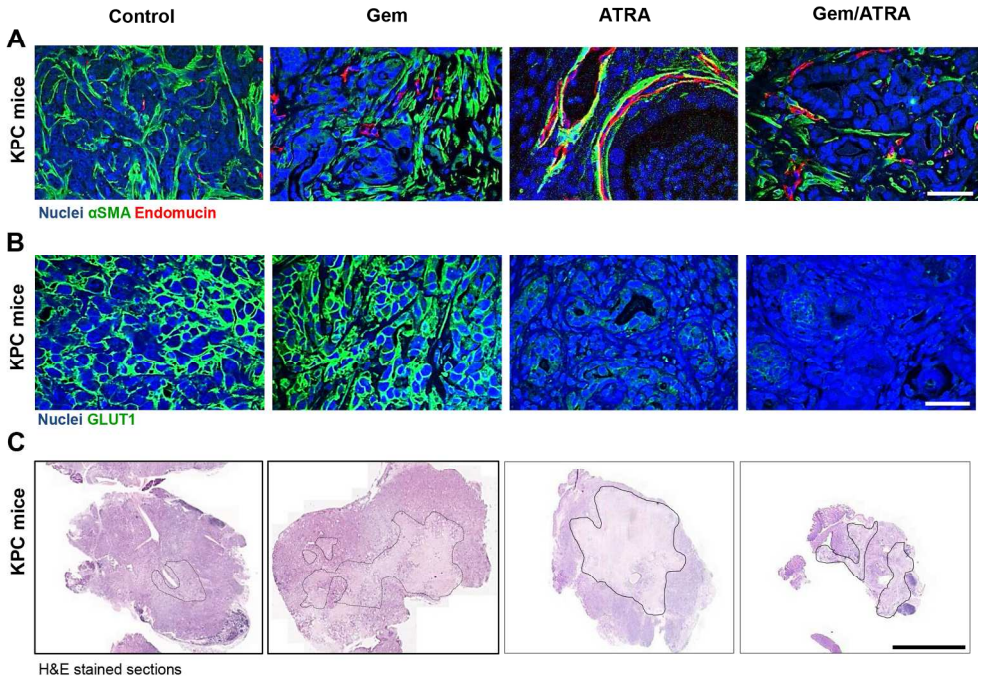

189x141mm (300 x 300 DPI)

Supplementary Figure 7

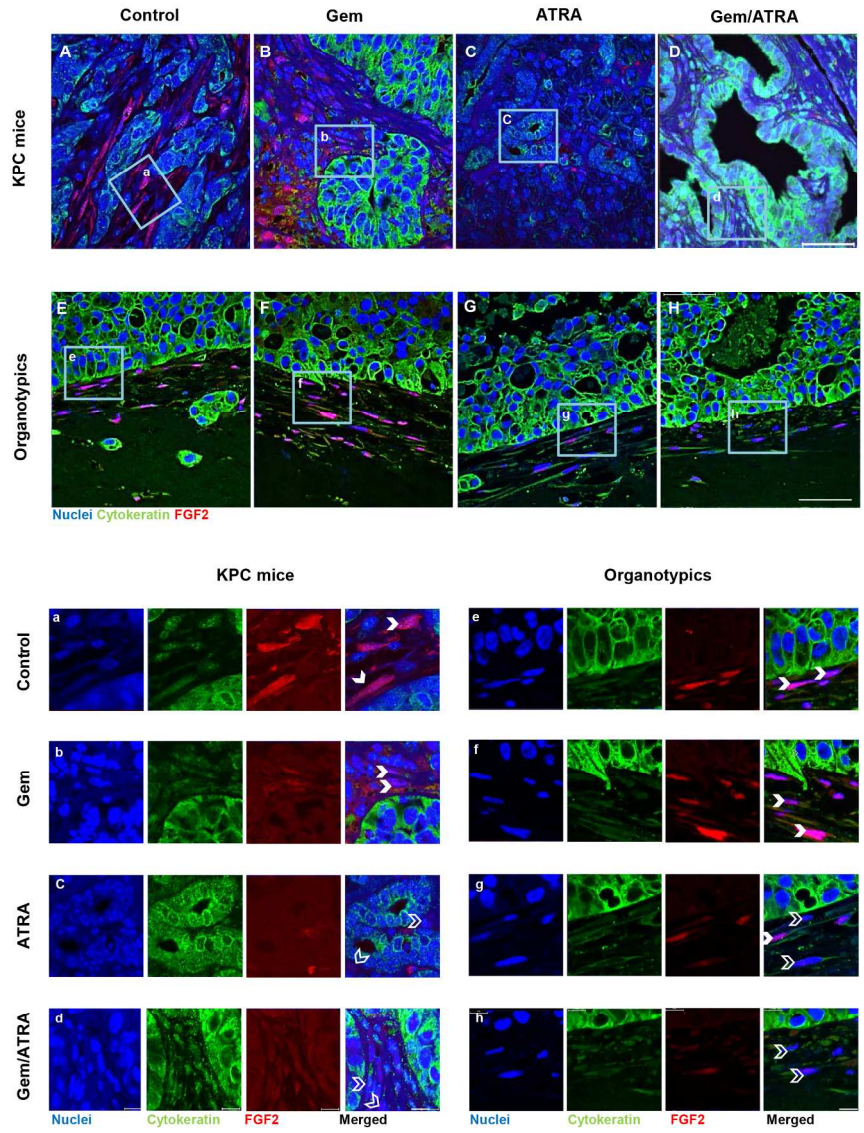

185x252mm (300 x 300 DPI)

Supplementary Figure 8

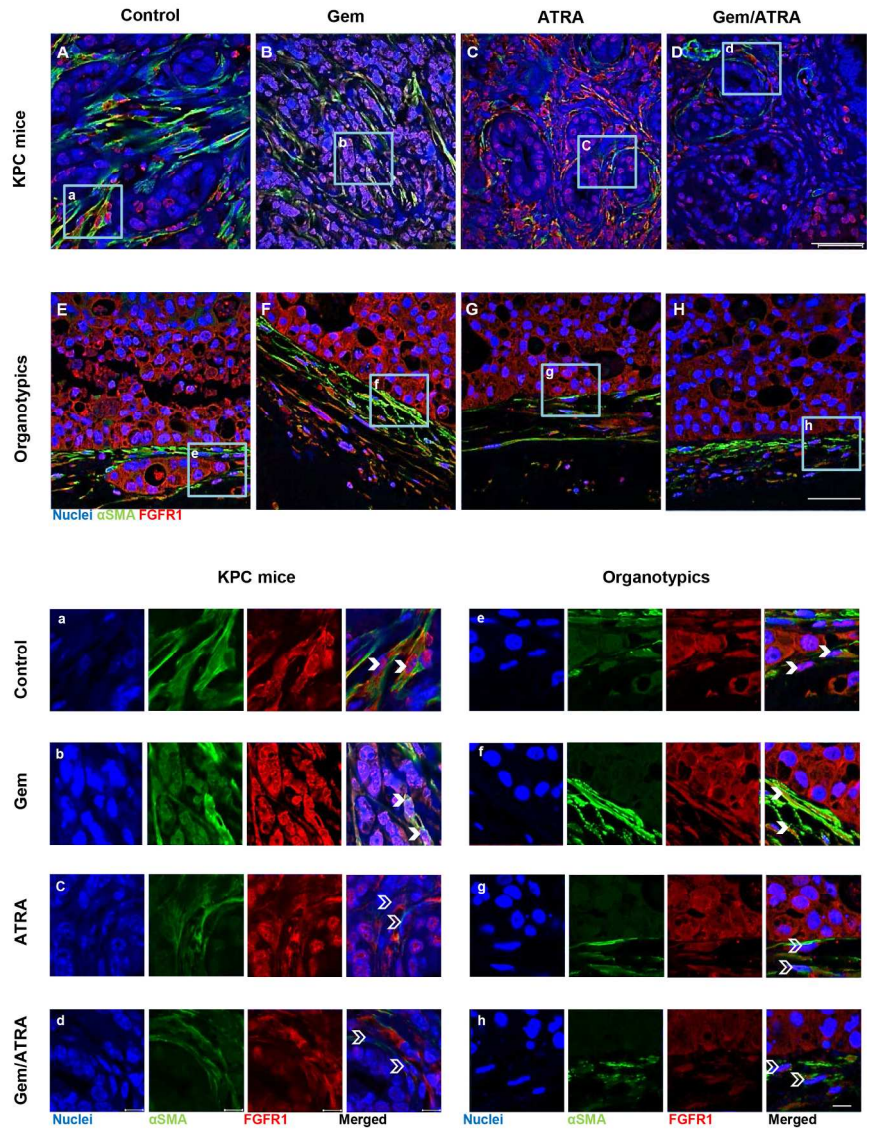

186x251mm (300 x 300 DPI)

Supplementary Figure 9

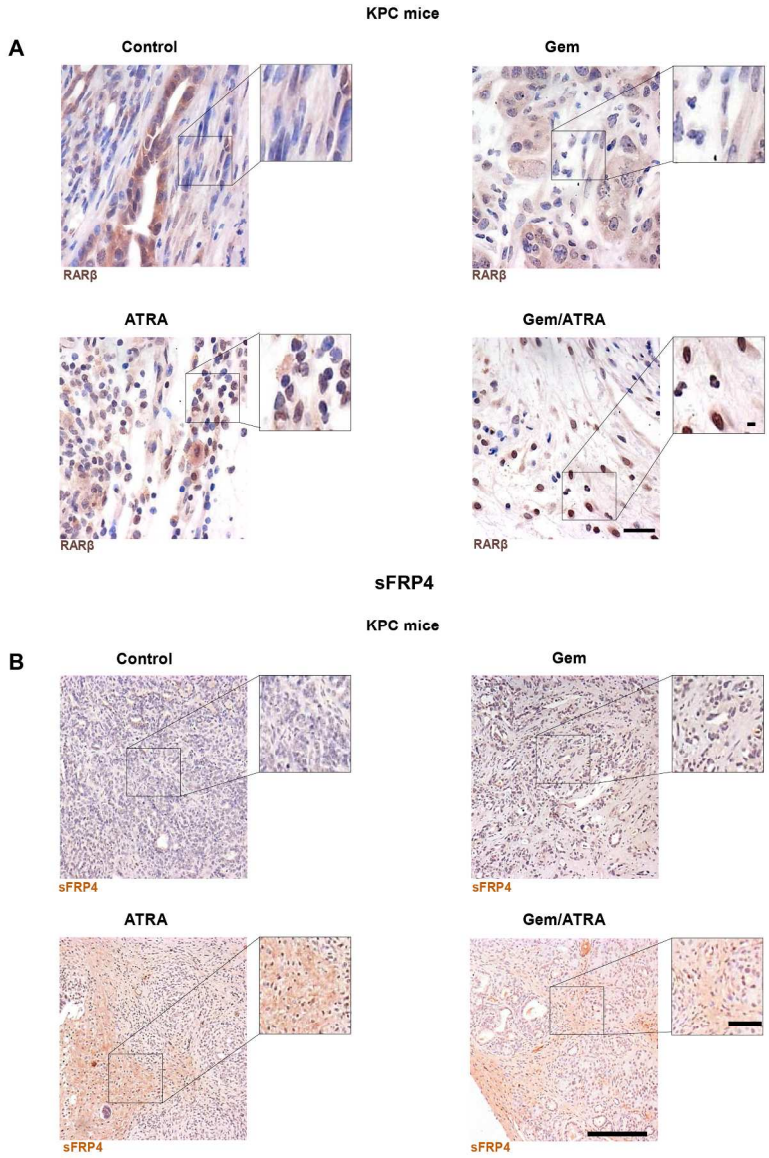

175x267mm (300 x 300 DPI)

Supplementary Figure 10

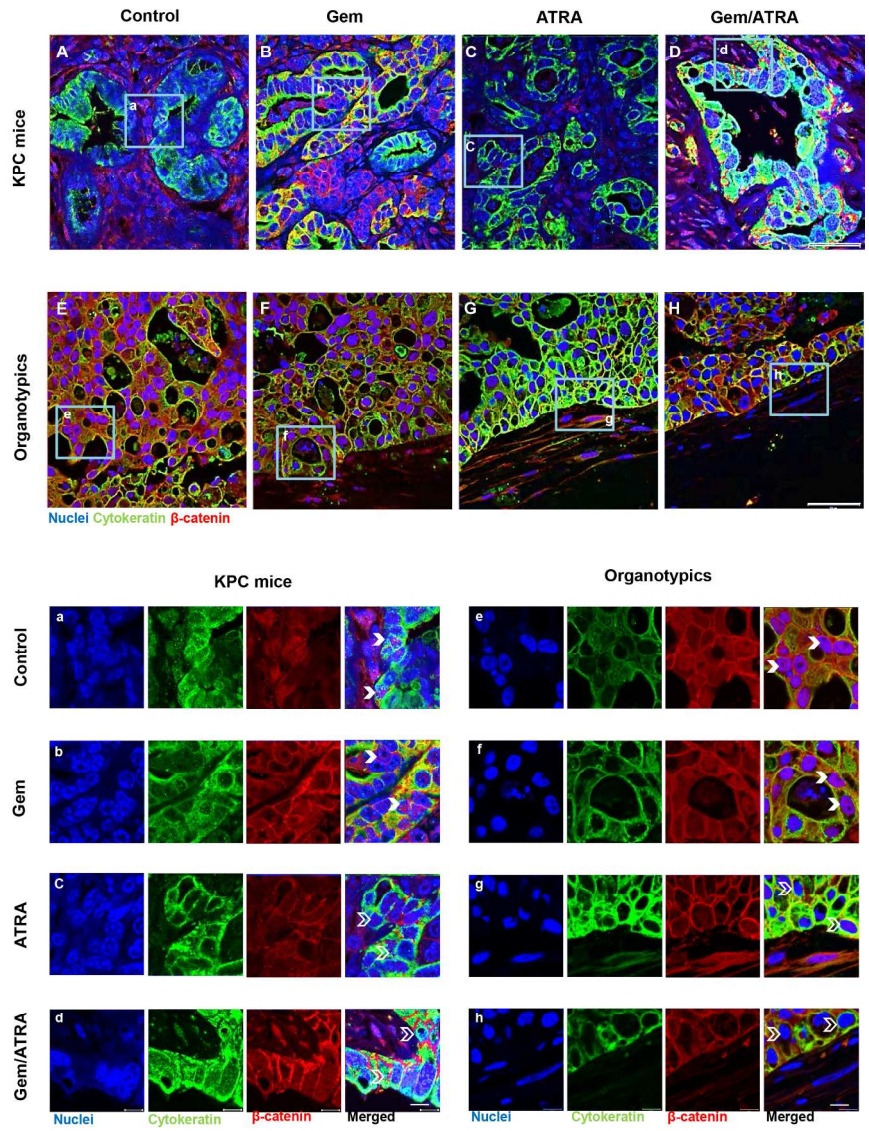

186x252mm (300 x 300 DPI)

Supplementary Figure 11

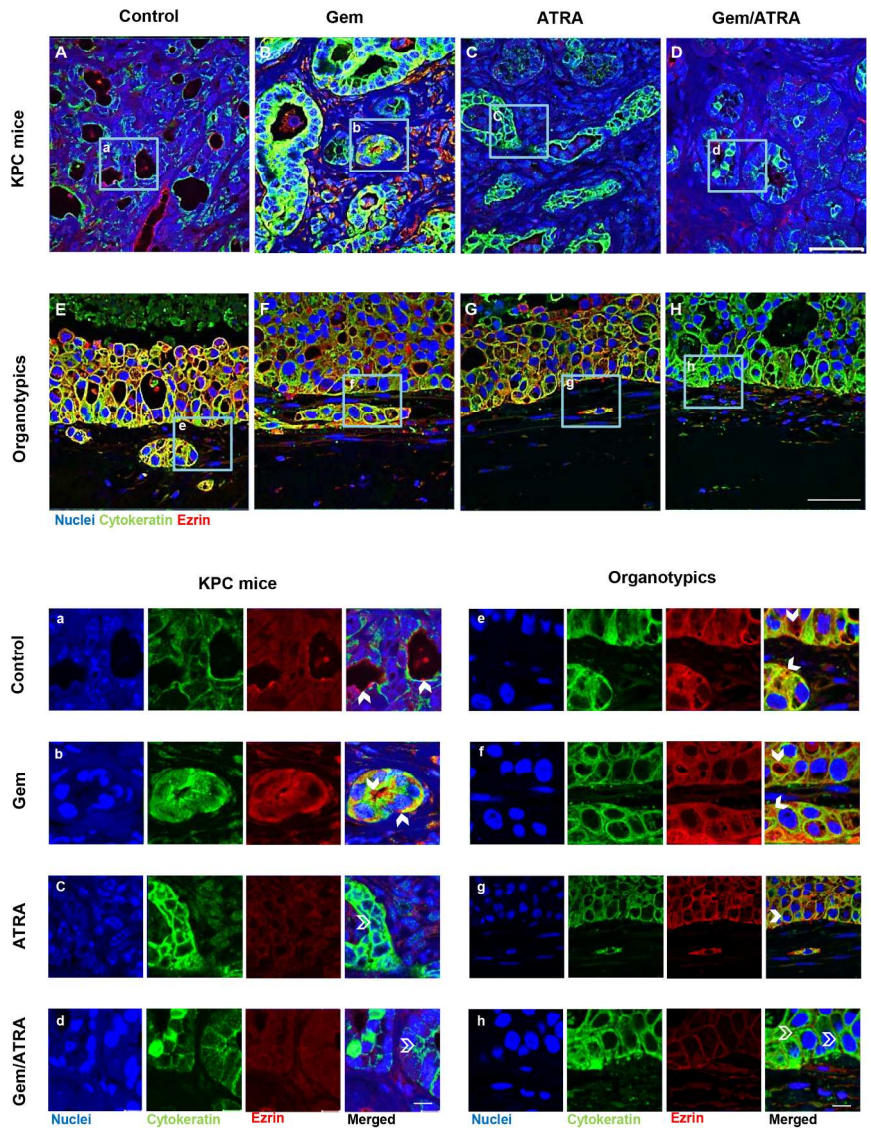

186x251mm (300 x 300 DPI)

Supplementary Figure 12

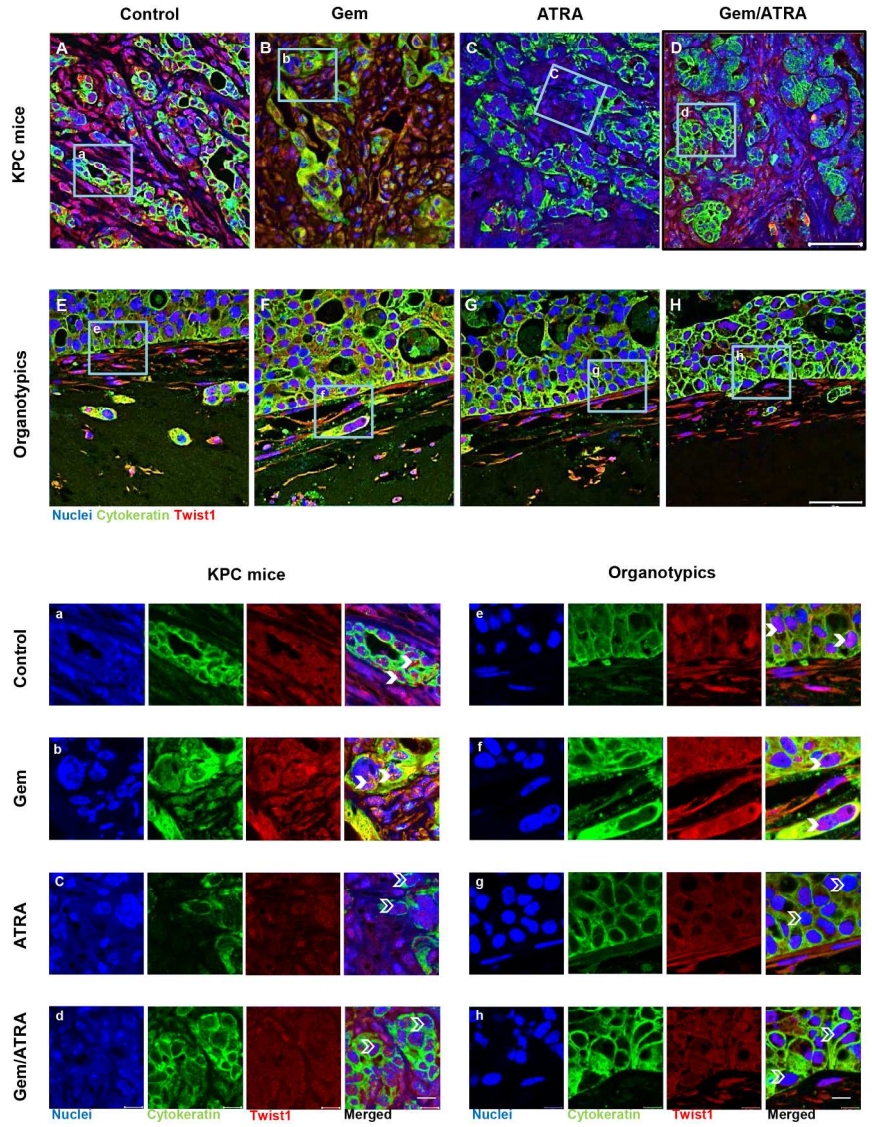

186x251mm (300 x 300 DPI)

Supplementary Figure 13

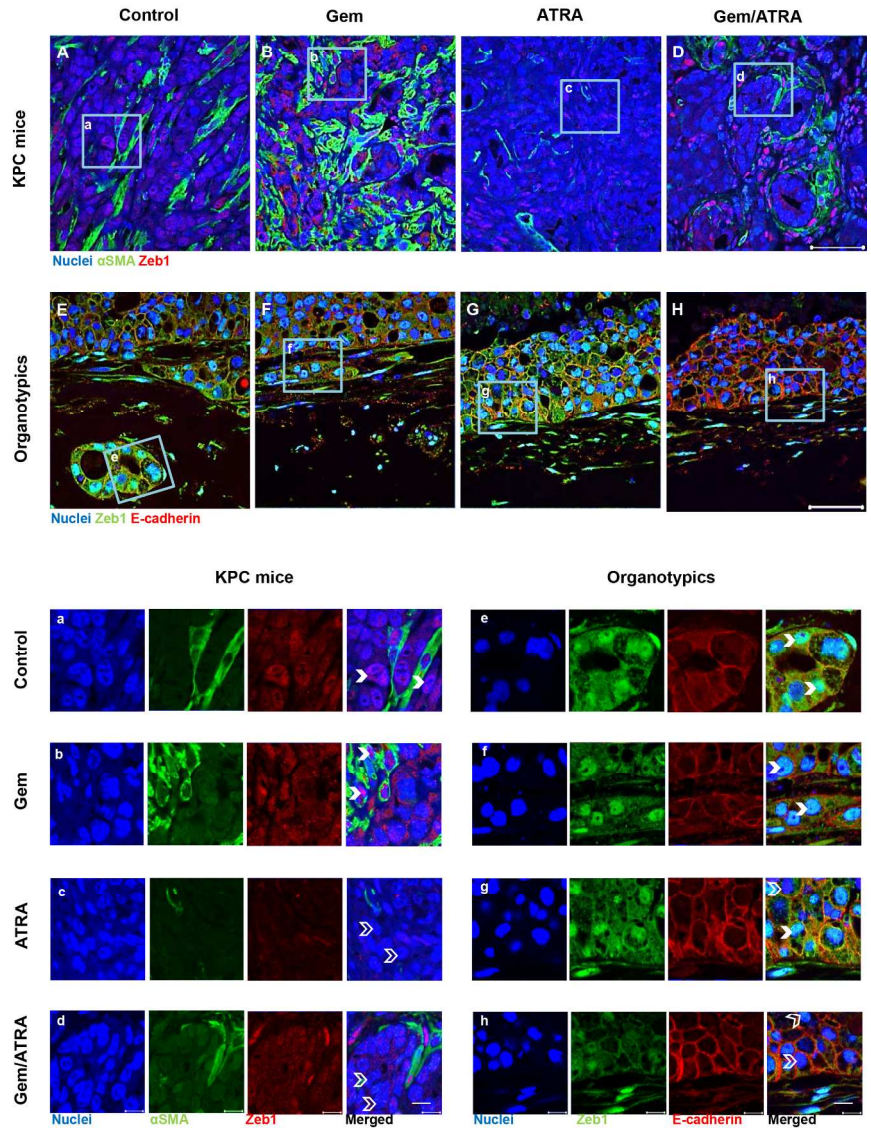

186x252mm (300 x 300 DPI)

Supplementary Figure 14

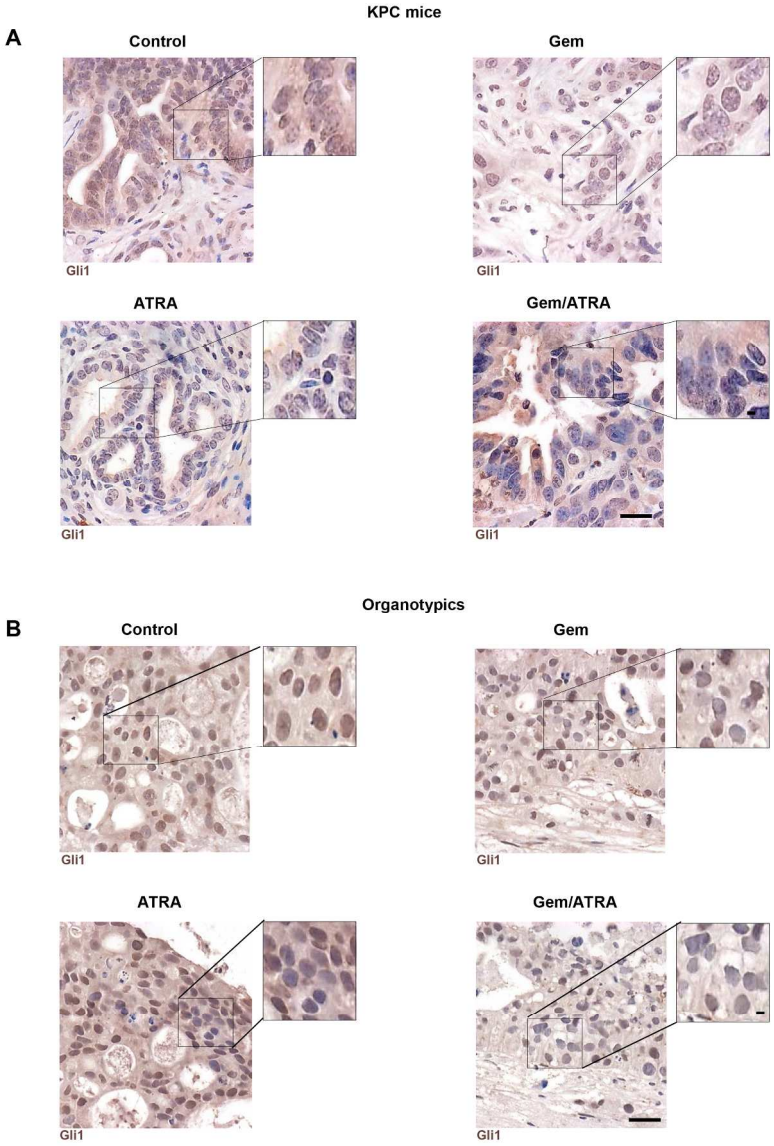

177x267mm (300 x 300 DPI)

Anti-stromal treatment together with chemotherapy targets multiple signalling pathways in pancreatic adenocarcinoma.

Elisabete F. Carapuça[1#], Emilios Gemenetzidis[1#], Christine Feig[2], Tashinga E. Bapiro[2], Michael D. Williams[2], Abigail S. Wilson[1], Francesca R. Delvecchio[1], Prabhu Arumugam[1], Richard P. Grose[1], Nicholas R. Lemoine[3], Frances M. Richards[2], Hemant M Kocher[1,4*]

[1]Centres for Tumour Biology and [3]Molecular Oncology, Barts Cancer Institute – a CRUK Centre of Excellence, Queen Mary University of London, London EC1M 6BQ, UK.

[2]The University of Cambridge Cancer Research-UK Cambridge ~~Research~~ Institute, Li Ka Shing Centre, Robinson Way Cambridge, CB2 0RE, England.

[4]Barts and the London HPB Centre, The Royal London Hospital, Barts Health NHS Trust, London, E1 1BB, UK.

Running head: stroma and cancer co-targeting

***Corresponding author:** Hemant M Kocher MS MD FRCS, Queen Mary University of London, Centre for Tumour Biology, Barts Cancer Institute and CR-UK Clinical Centre, Barts & The London School of Medicine & Dentistry, Charterhouse Square, London EC1M 6BQ. UK.

Tel: +44(0) 20 7882 3579 Fax: +44(0) 20 7882 3884

Email: h.kocher@qmul.ac.uk

Disclosures: All authors have nothing to disclose.

#Contributed equally

Key words: Gemcitabine, all-trans-retinoic acid, quiescence, pancreatic stellate cells, Collagen, fibronectin.

Total word count: ~~5785~~ 3187 Abstract word count: 260

Figures: 6 Supplementary Figures: 14 References: 40

Grant Support:

This work was supported by project grants from the Knowledge Transfer Network (Engineering and Physical Sciences Research Committee) and Pancreatic Cancer Research Fund (UK) to HMK. CF was supported by an EMBO long term fellowship and by a Marie Curie Intra-European Fellowship within the 7th European Community Framework Programme. TB and FR were supported by Cancer Research UK (grant C14303/A17197). Other grant funding includes project grants from Pancreatic Cancer Research Fund, Cancer Research UK and Barts Charity.

Acknowledgements:

This manuscript is dedicated to both parents of EFC, who sadly died during the study period. We thank members of the Kocher laboratory (Centre for Tumour Biology) for criticism and suggestions throughout this project. We thank Professor Ian Hart for comments on the manuscript. We thank Professor David A Tuveson (Cambridge Research Institute and Cold Spring Harbor Laboratory) for his critical insight and provision of KPC mice.

Author contributions:

Study concept, design and supervision and obtained funding: HMK; acquisition of data: EFC, EG, CF, MDW, TEB, ASW, FRD, PA, HMK; statistical analysis: EFC, HMK; drafting of the manuscript: HMK, EFC; technical or material support: RPG, FMR, NRL, HMK; analysis and interpretation of data as well as critical revision of the manuscript for important intellectual content: all authors.

Abbreviations:

ATRA: All-Trans Retinoic Acid;

BMP: bone morphogenetic protein;

FBS: Fetal Bovine Serum;

FGF: fibroblast growth factor;

FGFR: fibroblast growth factor receptor;

KPC: *LSL-Kras*$^{G12D/+}$*; LSL-Trp53*$^{R172H/+;}$ *Pdx-1-Cre*;

LC-MS: Liquid chromatography–mass spectrometry;

PDAC: Pancreatic Ductal Adenocarcinoma;

PSC: Pancreatic Stellate Cells;

RA: Retinoic Acid;

RARβ: Retinoic acid Receptor β;

SHH: sonic hedgehog;

STR: Short tandem repeat;

TGFβ: transforming growth factor β;

Abstract

Background & Aims: Stromal targeting for pancreatic ductal adenocarcinoma (PDAC) is rapidly becoming an attractive option, due to lack of efficacy of standard chemotherapy and increased knowledge about PDAC stroma. We postulated that combining stromal therapy may enhance anti-tumour efficacy of chemotherapy.

Methods: Gemcitabine and all-*trans* retinoic acid (ATRA) were combined in a clinically applicable regimen, to target cancer cells and pancreatic stellate cells (PSC) respectively, in 3D organotypic culture models and genetically engineered mice (*LSL-Kras*$^{G12D/+}$*;LSL-Trp53*$^{R172H/+}$*;Pdx-1-Cre* mice: KPC mice) representing the spectrum of PDAC.

Results: In two distinct sets of organotypic models as well as KPC mice, we demonstrate a reduction in cancer cell proliferation and invasion together with enhanced cancer cell apoptosis when ATRA is combined with Gemcitabine compared to vehicle or either agent alone. Simultaneously, PSC activity ÷ (in the form of deposition of extra-cellular matrix proteins such as Collagen and Fibronectin), and PSC invasive ability were both diminished in response to combination therapy. These actions were mediated by affecting a range of signalling cascades (Wnt, hedgehog, retinoid and FGF were studied) in cancer as well as stellate cells, effecting myriad epithelial cellular functions such as epithelial-mesenchymal transition, cellular polarity and lumen formation. At the tissue level, this resulted in enhanced tumour necrosis, increased vascularity, and diminished hypoxia. Consequently, there was an overall reduction in tumour size.

Conclusions: Stromal co-targeting (ATRA) alongside chemotherapy (Gemcitabine) is a potential clinical strategy. Experimental evidence suggests that the effect of this combination is mediated by dampening multiple signalling cascades in the tumour-stroma cross-talk, rather than ablating stroma or targeting a single pathway.

Introduction

Combination chemotherapy regimens consisting of oxaliplatin, irinotecan, fluorouracil, and leucovorin (FOLFIRINOX) [1] or nab-Paclitaxel with Gemcitabine [2] have resulted in increased median overall survival compared to Gemcitabine alone, which is the currently approved and widely used palliative mono-therapy [3]. However, gains have been marginal, and this may well be because desmoplasia remains largely unaltered with therapy[4].

PDAC is characterised by a pronounced desmoplastic stroma mediated by the activation of quiescent pancreatic stellate cells (PSC) [5]. This stroma creates a uniquely hypoxic microenvironment that, paradoxically, promotes both tumour growth and metastatic spread while inducing vascular collapse, thus creating a barrier to the perfusion/diffusion of therapeutic agents[6]; which, altogether, makes this cellular desmoplastic stroma an appealing therapeutic target. The pharmacologic inhibition of the sonic hedgehog signalling pathway in combination with Gemcitabine, in a genetically engineered mouse model, *LSL-Kras$^{G12D/+}$;LSL-Trp53$^{R172H/+}$;Pdx-1-Cre* (KPC) mice, produced variable results dependent on disease stage [7, 8], yet demonstrated proof-of-concept that stromal targeting was feasible. However, stromal ablation leads to a biologically more aggressive form of PDAC [8, 9], indicating that attention to the spatio-temporal aspects[4] of the tumour-stroma cross-talk is critical for its effective targeting [10].

PSC play a central role in desmoplastic stroma [11, 12]. Previously, we demonstrated that restoring the quiescent state of PSC, by replenishing their physiological retinol depots using the pleiotropic agent: all-trans retinoic acid (ATRA), halted tumour progression through targeting multiple dynamic tumour-stromal signalling cascades [13, 14]; a notion recently supported by targeting Vitamin D receptor [15]. In this report, we used combination therapy to target pancreatic cancer cells and their supporting stroma in *in vitro* and *in vivo* PDAC models to demonstrate efficacy of this strategy. It is feasible to target and normalize multiple altered signalling cascades mediating tumour-stroma cross-talk with this approach.

Methods

Organotypic cultures:

Short tandem repeat (STR) profiled cancer (Capan1, AsPC1) and stellate (PS1) cells were cultured, and pancreatic organotypic cultures were constructed as described elsewhere [11, 16-18]. Two cancer cell lines were utilised in organotypic models representing a spectrum of PDAC differentiation[11, 13, 18]. The pancreatic stellate cell line used was PS1, which was obtained from an unused normal pancreas (rejected for transplantation) donated by the UK human tissue bank (Ethics approval; Trent MREC (/MRE04/)). The cells were isolated in the laboratory, using the outgrowth method [19, 20] followed by immortalisation by expression of ectopic human telomerase reverse transcriptase (hTERT) [21], and verified as being of stellate cell origin by positive immunostaining for Desmin, Vimentin, αSMA and GFAP and ability to store Vitamin A [13].

In contrast to previous reports [13, 17], we allowed the cancer-stellate interaction to be established for 10 days [11], before commencing therapeutic dosing, for the treatment of an established tumour analogue. The cancer cell: stellate cell ratio was 1:2, as determined previously, providing the most aggressive, invasive phenotype within this model which mimicked histological features of advanced human cancer [11]. Multiple biological and technical replicates performed by two independent researchers ensured reproducibility. Treatment was given for two cycles, as per the human clinical protocol [3, 22], ~~as summarized in Supplementary Figure 1~~. Briefly, treatment of organotypic cultures was performed daily with ATRA (Sigma R2625, St. Louis, MO, USA) at 1μM or with weekly Gemcitabine (2', 2'-difluoro 2'-deoxycytidine, dFdC) (Eli Lilly, Indianapolis, IN, USA) at 100 nM (Capan-1/PS1) or 400 nM (AsPC1/PS1), or with the combination of Gemcitabine/ATRA or with respective vehicles. Organotypic cultures were harvested on day 24, fixed in 10% neutral buffered formalin (Cell Pathology BAF-001003A, Newton, UK), embedded in paraffin and cut into 4

μm sections. Each experiment had three technical replicates and at least three biologic repeats.

KPC mice treatment

All animal work was done in accordance with the UK Animals (Scientific Procedures) Act 1986, revised by the Amendment Regulations 2012 (SI 2012/3039) to transpose European Directive 2010/63/EU with approval from the local Animal Welfare and Ethical Review Body, and following the 2010 guidelines from the United Kingdom Coordinating Committee on Cancer Research [23]. Compound mutant KPC mice with mature, established tumours were enrolled at a median age of 180 days and used as described previously [7, 13]. ATRA was dissolved to 25mg/ml in dimethyl sulfoxide, further diluted to 2.98mg/ml in (2-Hydroxypropyl)-β-cyclodextrin (Sigma-Aldrich H5784) and finally to 1.5mg/ml with sterile filtered tap water. This ATRA solution was administered orally to mice at 15 mg/kg daily for seven days [13]. Gemcitabine was injected intraperitoneally at 100 mg/kg on days zero, three and seven [7]. The volume of the tumours was measured by ultrasound two days before the beginning of the treatment, and mice bearing tumour volume of ~250 mm^3 (Supplementary ~~**Figure 1**~~ Table 1) were selected for the study. Tumours were harvested seven days after beginning of the treatment, and immediately submerged in formalin for 24 hours, followed by embedding in paraffin blocks for further sectioning and immunostaining analysis. The primary endpoint of study was drug efficacy as measured by a number of surrogate markers. Samples of tumours and serum were also snap-frozen for analysis of drug concentrations using LC-MS/MS.

Immunostaining

Paraffin-embedded sections were dewaxed and re-hydrated, and antigens were retrieved and immunostained for a range of markers to study cellular attributes using a range of antibodies (Supplementary Table 2) as described before [13, 16].

Quantification

The quantification of all cell counts and intensity of staining in the organotypic sections was performed on four-six representative pictures per organotypic gel of which there were three technical replicates for each of the biological repeats (minimum three). For the KPC mice, either the total tumour area or at least ten representative pictures per total tumour area were scanned using either Axioplan microscope (Zeiss 40 V 4.8.10, Carl Zeiss MicroImaging LLC, New York, US), confocal laser scanning microscope LSM 510 (Carl Zeiss MicroImaging LLC, New York, US) or Pannoramic 250 High Throughput Scanner (3DHISTECH Ltd., Budapest, Hungary). The intensities of fluorescence in the green/red channels were normalised with IgG controls and background fluorescence and calculated in an unbiased, blinded manner using either Adobe Photoshop CS6 (San Jose, CA USA), or Pannoramic Viewer Software (3DHISTECH Ltd., Budapest, Hungary), and Image J software (NIH, Maryland USA) as described before [13]. The methods for measurement of gel length and thickness, cancer and stellate total cell number per gel are described elsewhere [11].

Tissue Gemcitabine and ATRA levels

Tissue samples were homogenized in 50% acetonitrile:water at a concentration of 100 mg/mL using a precellys homogenizer. An aliquot of the homogenate was precipitated with acetonitrile containing a stable isotope (5 deuterium) label internal standard of ATRA. Measurement was carried out against a calibration line prepared in mouse plasma homogenate (100 mg/mL) in 50% acetonitrile:water. The MS/MS used was a Sciex 4000Qtrap equipped with a heated nebulizer atmospheric pressure chemical ionization source operating in the negative mode at 350ºC. MRM transitions were 301-205 and 306-205 for unlabeled and labeled ATRA respectively. LC was performed using a Dionex Ultimate 3000 LC and autosampler, using a gradient separation on a Phenomenex Kinetex 2.6 µm, 150x2.1 mm column. The binary gradient was run at 0.2 ml/min, starting at 40:60

A:B changing to 10:90 A:B from 0-15mins then holding from 15-17.6 minutes before quickly ramping back to 40:60 A:B at 17.62 minutes. The LC-MS/MS system was controlled by Analyst 1.4 software. In order to ensure the correct isomer (ATRA) was measured a system suitability test was run at the beginning and end of the sample analysis to demonstrate separation of the ATRA isomer from the 9- and 13-cis isomers of retinoic acid (data not shown). ~~**(Supplementary Figure 7).**~~

Fresh frozen tumour and plasma samples were processed and analysed for Gemcitabine and its metabolites by LC-MS/MS as previously described [24]. Briefly, LC-MS/MS was performed on a TSQ Vantage triple stage quadrupole mass spectrometer (Thermo Scientific, USA) fitted with a heated electrospray ionization (HESI-II) probe operated in positive and negative mode at a spray voltage of 2.5 KV, capillary temperature of 150ºC. Quantitative data acquisition was done using LC Quan2.5.6 (Thermo Fisher Scientific, USA).

Statistical analysis

Statistical analysis and graphical data representation were performed using the software PRISM V.6 (Graphpad, La Jolla, USA). Summary data are expressed as the median with interquartile range since the distribution was non-Gaussian. Comparisons were performed using Kruskal-Wallis test with Dunn's multiple comparison test. The level of significance was set at $P < 0.05$.

Results

Dosing schedule and timing for treatment of organotypic cultures and KPC mice with Gemcitabine and ATRA were designed to mimic clinically relevant treatment regimens for advanced human pancreatic cancer based on previously available data [3, 7, 11, 13, 22]. *In vitro* optimisations such as growth inhibition to 50% of control (GI_{50}) levels for Gemcitabine were determined for translation into the organotypic 3D model.~~and summarized in Supplementary Figure 1~~.. Interestingly, we found the presence of extra-cellular matrix (ECM) protein in 3D model to have preferential cytoprotective effect on the pancreatic stellate cells (PSC). This resulted in different GI_{50} for both PSC and cancer cells in 3D models compared to 2D culture (Supplementary Figures 1~~A-C~~, data not shown). Previously we had demonstrated ATRA had no direct effect on cancer cells by performing PSC or cancer cell alone organotypic cultures [13].

~~Mice were enrolled independently and randomly allocated into the trial at advanced stage based on ultrasound (Supplementary Table 1 [7]).~~ We then sought to identify effects on the cancer cells and stellate cells separately within this experimental design mimicking advanced PDAC. ~~Results are presented across all biological replicates using a fold change for various attributes measured as summarized in Supplementary Figures 2 and 3.~~ There was no change in gel contractility in organotypic cultures with any of the agents as compared to vehicle treatment (Supplementary Figure 2 ~~and 3~~).

There was a significant reduction in proliferation of cancer cells induced by the presence of ATRA either alone or in combination with Gemcitabine *in vivo* as well as *in vitro*, across all experimental conditions (Figures 1A-C, Supplementary Figures **4**3A ~~**4B**~~ and B).No significant difference was noted for stellate cells proliferation after any of the treatments (Supplementary Figure 3C). However, induction of apoptosis was more pronounced with introduction of ATRA in the combination arm, suggesting that Gemcitabine potentiates the effect of ATRA (Figures 1D-F, Supplementary Figure ~~**4C**~~3D and E). We did not find any significant difference in the apoptotic index of stellate cells after any of the treatments, in

both PDAC models (Supplementary Figure 3F). Cancer cell invasion into the extra-cellular matrix, a surrogate marker for metastatic capability, was also reduced by the combination treatment (Figures 2A-B, Supplementary Figure 4A-B).

PSC invasion into the ECM, and stellate cell density in mouse tumours, were reduced by ATRA treatment alone, and in combination with Gemcitabine (Figures 2C-E, Supplementary Figures 4A-C). PSC numbers within organotypic gels did not change, reflecting the protective effect of matrix proteins on PSC in 3D, not seen in 2D *in vitro* state (Supplementary Figures 1B and 2D-E). However, the PSC activation state was altered by ATRA and the combination of Gemcitabine and ATRA, as indicated by a significant reduction in deposition of extra-cellular matrix (ECM) substrates such as Fibronectin and Collagen I, implying stromal re-modelling (Figures 3A-D, Supplementary Figures 5A-C).

Together with stromal re-modelling, we demonstrated increased vascularity of the KPC tumours, associated with decreasing hypoxia (Figures 3E, 3F, Supplementary Figures 6A, 6B). Surprisingly, despite this reduction in hypoxia, there was increased necrosis, *in vivo*, with combination treatment (Figure 4A~~),,~~ Supplementary Figure 6C). This resulted in smaller tumours in mice treated with combination therapy (Figure 4B). Certainly, with this regimen, both agents can be delivered successfully *in vivo* into the tumour parenchyma as measured by LC-MS/MS (Figures 4C-E). Furthermore, the tissue ATRA (not 9-cis and 13-cis RA) is directly correlated to serum ATRA measurements allowing surrogate measurements to be easily and readily performed (Figure 4C~~, Supplementary Figures 7C, 7D).~~

The precise mechanism(s) underpinning the success of this combination therapy are difficult to pinpoint, since ATRA influences multiple signalling cascades [13]. The enhanced apoptosis and reduction in proliferation of cancer cells may result from the reduction of Wnt signalling in the tumour compartment [13], disrupted fibroblast growth factor (FGF) signalling in the stromal compartment [17], or targeting of other signalling cascades such as Hedgehog, IL6, and CXCL12 amongst others [14].

In our experimental models, we could demonstrate a reduction in nuclear translocation of FGF2 and FGFR1 in PSC upon treatment of KPC mice and organotypic

cultures with ATRA (Figures 5A-F, Supplementary Figures 7,8); this co-translocation being pertinent to PSC activity as demonstrated before [13]. There was enhanced nuclear Retinoic Acid Receptor β (RARβ) visibility within the PSC in KPC tumours upon treatment with ATRA ~~treatment~~ (Figure 5G, Supplementary Figure 9A), which is known to reflect PSC quiescence [13]. Upregulation of PSC RARβ activity enhances secretion of secreted Frizzled related protein 4 (sFRP4) from the quiescent PSC as demonstrated before [13]. We could demonstrate increased stromal sFRP4 upon treatment with ATRA (Figure 5H, Supplementary Figure 9B). This modulation within PSC upon treatment with ATRA, in turn, led to reduced nuclear β-catenin, which ~~is normally trans-located~~ translocates to the nucleus following canonical Wnt signalling activation [13, 25] (Figure 6A, Supplementary Figure 10). sFRP4 can sequester Wnt ligands within stroma to abrogate canonical Wnt signalling flux, and also act as gatekeeper, and, thus, affect epithelial-mesenchymal transition (EMT), apoptosis and invasion within cancer cells [26, 27].

In addition, there was reduction in Ezrin expression (Figure 6B, Supplementary Figure 11), which has previously been shown to enhance podosomal rosette formation [25]. Ezrin is also a marker for lumen formation and apico-basal polarity and such changes could be observed in the organotypic cultures more clearly than KPC mice but were difficult to quantify (data not shown). Furthermore, there was suppression in the expression of EMT activating transcription factors, as evidenced by reduction of nuclear *Twist1* and *Zeb1* in PDAC cells (Figures 6C and D, Supplementary Figures 12, 13), which may be related to reduction of canonical Wnt signalling [28]. Lastly, there was also reduction of nuclear and cytoplasmic Gli1 in cancer cells, suggesting reduced Hedgehog signalling in cancer cells [29] (Figure 6E, Supplementary Figure 14). The alteration of the vascular and immune sub-compartments of stroma, as shown by us before[14, 30], could also lead to enhanced necrosis in tumours *in vivo*, especially with combination treatment, ultimately resulting in tumour shrinkage.

Discussion

The effective ~~reduction of~~ reduced growth of the tumour size with a combination of stromal and cancer cell co-targeting is clinically relevant, since many locally advanced and borderline resectable cancers may be rendered surgically resectable using this regimen, a hypothesis which is now ready to be tested in clinical trials. The findings reported here are in sharp contrast to two recent studies exploring more radical approaches involving complete stromal ablation [8, 9] suggesting that stromal "normalisation" is much preferable over stromal ablation approaches [10]. Rhim et al, recently demonstrated that ablating sonic hedgehog-dependent stroma resulted in a more vascular tumour with poor differentiation, which, in part, could be abrogated by VEGF signalling blockade [8]. In a parallel approach, Ozdemir et al, by genetically ablating alpha-SMA-positive stroma, demonstrated presence of more invasive tumours, characterized with hypoxia, an epithelial-to-mesenchymal transition and alterations in immune surveillance. Specifically, this resulted in increased $CD4^{+}Foxp3^{+}$ T-regulatory cell infiltration, leading to a more aggressive tumour phenotype [8, 9]. In contrast, our findings suggest that restoring homeostatic stromal characteristics, rather than stromal ablation, have tumour-suppressive rather than a tumour-enhancing effect. This may be, in part, due to the homeostatic role of naturally occurring vitamin A analogue, and, in part, due to the pleiotropic actions of ATRA which are of relevance to pancreatic embryology and development.

Indeed, it has been demonstrated that ATRA influences multiple signalling cascades through selective retinoid receptor signalling (retinoid versus rexinoid receptors and isoforms of both subsets such as α,β,γ) in embryonic pancreas development, injury and regeneration [13, 31-34]. In particular, ATRA has a predominant effect on acinar morphology rather than endocrine cells, due to the epithelial-mesenchymal interactions in the developing pancreas [34]. Retinoic acid is critical for the developing pancreas, where it can interact with, and influence Wnt, TGFβ (transforming growth factor β), BMP (bone morphogenetic protein), and other signalling cascades [35], all of which are understood to be hijacked and altered by

cancer cells to recruit stromal cells [36]. Previously we had demonstrated that restoring the quiescent nature of PSC using ATRA can alter the signalling flux within the tumour-stroma [13] as well as intra-stromal cross-talk [14] of key pathways relevant to pancreatic cancer progression.

The enhanced apoptosis and reduction in proliferation of cancer cells, seen in this report, may result from reduction of canonical Wnt signalling in the tumour compartment, as a result of modification in the stromal compartment, by sequestering Wnt ligands, due to sFRP4 secretion [13]. Furthermore the disrupted fibroblast growth factor (FGF) signalling in the stromal compartment [17], or targeting of other signalling cascades such as Hedgehog, IL6, CXCL12 amongst others [14], could detrimentally effect the cancer cells by altering the signalling flux of, rather than selectively ablating, key cascades. FGF2/FGFR1 nuclear translocation is vital to activation of PSC which is required for cancer progression, as recently shown by us [17]. ~~**CXCL12 signalling is vital in recruiting immune cells within the cancer micro-environment.**~~ Other modifications in extra-cellular matrix deposition and re-~~**modeling**~~ modelling such as Collagen and Fibronectin can affect the cyto-protective micro-environment of cancer cells [37], internalisation and re-cycling of key integrins [18] and migration/invasion of cancer cells [38] as well as immune cells [14].

This alteration of a number of signalling pathways, in turn, may affect key epithelial cellular processes such apico-basal polarity [25], matrix re-modelling [18], epithelial-mesenchymal transition [26] and, thus, halt cancer progression. Therefore, multiple tumour-stroma cross-talk signalling cascades affecting numerous cancer and stellate cell processes are altered by ATRA when administered in clinically achievable dosing schedule.

Moreover, the alteration of immune cell infiltrate, vascularity and hypoxia demonstrated by us previously [13, 14, 30] in relation to stromal targeting therapy is relevant to this combination treatment. We demonstrate, here, that chemotherapy is more effective when combined with ATRA in altering intra-stromal or peri-tumoural cross-talk in the tissue micro-environment, particularly the enhancement of vascularity and the consequent reduction in hypoxia. In fact, it has been long understood that the tumour micro-environment

exerts a protective influence on the cancer cells through multiple mechanisms such as resistance to alkylating agents [39], direct cell-cell contact between cancer and stromal cells [40], through many signalling cascades, thus enhancing the tumour cell autonomous resistance to chemotherapy. We were unable to detect enhanced levels of active metabolite of Gemcitabine, and we speculate this may be related to increased necrotic component of the tumour which will not contain active metabolite. In addition, the consistency of the results obtained from these two different PDAC models (one *in vitro*, one *in vivo*) suggests that the organotypic models may be useful preclinical tools for dissection of the molecular signalling pathways involved in PDAC drug resistance. Modulating the 3D OT cultures would recapture important aspects of the tumour microenvironment that can influence cancer cell behaviour.

Thus, based on data presented here, we postulate that the effect of this combination strategy of co-targeting cancer and stromal cells is more likely to involve dampening of a multitude of signalling cascades, rather than via a single, specific pathway or mechanism and, therefore, altering a number of key cellular processes. This notion ~~agrees~~ concurs with separate attempts to restore homeostatic capability of desmoplastic stroma by targeting the vitamin D receptor [15], as well as normalisation of vascularisation with dual-action combination therapy [30]. Given the known fat-soluble vitamin deficiency in patients with PDAC, due to biliary and pancreatic duct obstruction, the proposal to restore homeostatic stromal function, in conjunction with cancer targeting with conventional chemotherapy, appears to be a viable therapeutic opportunity underpinned by the clinical features of this cancer. This hypothesis, thus, has enough rationale to be explored in a human clinical trial involving patients with PDAC.

.

References

1. Conroy T, Desseigne F, Ychou M, et al. FOLFIRINOX versus gemcitabine for metastatic pancreatic cancer. N Engl J Med 2011;364:1817-25.
2. Von Hoff DD, Ervin T, Arena FP, et al. Increased survival in pancreatic cancer with nab-paclitaxel plus gemcitabine. N Engl J Med 2013;369:1691-703.
3. The use of gemcitabine for the treatment of pancreatic cancer (TA25). National Institute for Health and Clinical Excellence. 2001.
4. Neesse A, Algul H, Tuveson DA, et al. Stromal biology and therapy in pancreatic cancer: a changing paradigm. Gut 2015;64:1476-84.
5. Neesse A, Michl P, Frese KK, et al. Stromal biology and therapy in pancreatic cancer. Gut 2011;60:861-8.
6. Provenzano PP, Cuevas C, Chang AE, et al. Enzymatic targeting of the stroma ablates physical barriers to treatment of pancreatic ductal adenocarcinoma. Cancer Cell 2012;21:418-29.
7. Olive KP, Jacobetz MA, Davidson CJ, et al. Inhibition of Hedgehog signaling enhances delivery of chemotherapy in a mouse model of pancreatic cancer. Science 2009;324:1457-61.
8. Rhim AD, Oberstein PE, Thomas DH, et al. Stromal elements act to restrain, rather than support, pancreatic ductal adenocarcinoma. Cancer Cell 2014;25:735-47.
9. Ozdemir BC, Pentcheva-Hoang T, Carstens JL, et al. Depletion of carcinoma-associated fibroblasts and fibrosis induces immunosuppression and accelerates pancreas cancer with reduced survival. Cancer Cell 2014;25:719-34.
10. Froeling FE, Kocher HM. Homeostatic restoration of desmoplastic stroma rather than its ablation slows pancreatic cancer progression. Gastroenterology 2015;148:849-50.
11. Kadaba R, Birke H, Wang J, et al. Imbalance of desmoplastic stromal cell numbers drives aggressive cancer processes. J Pathol 2013;230:107-17.
12. Apte MV, Wilson JS, Lugea A, et al. A starring role for stellate cells in the pancreatic cancer microenvironment. Gastroenterology 2013;144:1210-9.
13. Froeling FE, Feig C, Chelala C, et al. Retinoic Acid-Induced Pancreatic Stellate Cell Quiescence Reduces Paracrine Wnt-beta-Catenin Signaling to Slow Tumor Progression. Gastroenterology 2011;141:1486-97.
14. Ene-Obong A, Clear AJ, Watt J, et al. Activated pancreatic stellate cells sequester CD8+ T cells to reduce their infiltration of the juxtatumoral compartment of pancreatic ductal adenocarcinoma. Gastroenterology 2013;145:1121-32.
15. Sherman MH, Yu RT, Engle DD, et al. Vitamin d receptor-mediated stromal reprogramming suppresses pancreatitis and enhances pancreatic cancer therapy. Cell 2014;159:80-93.
16. Coleman SJ, Watt J, Arumugam P, et al. Pancreatic cancer organotypics: High throughput, preclinical models for pharmacological agent evaluation. World J Gastroenterol 2014;20:8471-81.
17. Coleman SJ, Chioni AM, Ghallab M, et al. Nuclear translocation of FGFR1 and FGF2 in pancreatic stellate cells facilitates pancreatic cancer cell invasion. EMBO Mol Med 2014;6:467-81.
18. Li NF, Gemenetzidis E, Marshall FJ, et al. RhoC interacts with integrin alpha5beta1 and enhances its trafficking in migrating pancreatic carcinoma cells. PLoS One 2013;8:e81575.
19. Apte MV, Haber PS, Applegate TL, et al. Periacinar stellate shaped cells in rat pancreas: identification, isolation, and culture. Gut 1998;43:128-33.
20. Bachem MG, Schneider E, Gross H, et al. Identification, culture, and characterization of pancreatic stellate cells in rats and humans. Gastroenterology 1998;115:421-32.
21. Li NF, Kocher HM, Salako MA, et al. A novel function of colony-stimulating factor 1 receptor in hTERT immortalization of human epithelial cells. Oncogene 2009;28:773-80.

22. Burnett AK, Hills RK, Grimwade D, et al. Inclusion of chemotherapy in addition to anthracycline in the treatment of acute promyelocytic leukaemia does not improve outcomes: results of the MRC AML15 trial. Leukemia 2013;27:843-51.
23. Workman P, Aboagye EO, Balkwill F, et al. Guidelines for the welfare and use of animals in cancer research. Br J Cancer 2010;102:1555-77.
24. Bapiro TE, Frese KK, Courtin A, et al. Gemcitabine diphosphate choline is a major metabolite linked to the Kennedy pathway in pancreatic cancer models in vivo. Br J Cancer 2014;111:318-25.
25. Kocher HM, Sandle J, Mirza TA, et al. Ezrin interacts with cortactin to form podosomal rosettes in pancreatic cancer cells. Gut 2009;58:271-84.
26. Ford CE, Jary E, Ma SS, et al. The Wnt gatekeeper SFRP4 modulates EMT, cell migration and downstream Wnt signalling in serous ovarian cancer cells. PLoS One 2013;8:e54362.
27. Pohl S, Scott R, Arfuso F, et al. Secreted frizzled-related protein 4 and its implications in cancer and apoptosis. Tumour Biol 2015;36:143-52.
28. Garg M. Epithelial-mesenchymal transition - activating transcription factors - multifunctional regulators in cancer. World J Stem Cells 2013;5:188-95.
29. Briscoe J, Therond PP. The mechanisms of Hedgehog signalling and its roles in development and disease. Nat Rev Mol Cell Biol 2013;14:416-29.
30. Wong PP, Demircioglu F, Ghazaly E, et al. Dual-action combination therapy enhances angiogenesis while reducing tumor growth and spread. Cancer Cell 2015;27:123-37.
31. Colvin EK, Susanto JM, Kench JG, et al. Retinoid signaling in pancreatic cancer, injury and regeneration. PLoS One 2011;6:e29075.
32. Tulachan SS, Doi R, Kawaguchi Y, et al. All-trans retinoic acid induces differentiation of ducts and endocrine cells by mesenchymal/epithelial interactions in embryonic pancreas. Diabetes 2003;52:76-84.
33. Kobayashi H, Spilde TL, Bhatia AM, et al. Retinoid signaling controls mouse pancreatic exocrine lineage selection through epithelial-mesenchymal interactions. Gastroenterology 2002;123:1331-40.
34. Kadison A, Kim J, Maldonado T, et al. Retinoid signaling directs secondary lineage selection in pancreatic organogenesis. J Pediatr Surg 2001;36:1150-6.
35. Pearl EJ, Bilogan CK, Mukhi S, et al. Xenopus pancreas development. Dev Dyn 2009;238:1271-86.
36. Jones S, Zhang X, Parsons DW, et al. Core signaling pathways in human pancreatic cancers revealed by global genomic analyses. Science 2008;321:1801-6.
37. Mantoni TS, Lunardi S, Al-Assar O, et al. Pancreatic stellate cells radioprotect pancreatic cancer cells through beta1-integrin signaling. Cancer Res 2011;71:3453-8.
38. Lu J, Zhou S, Siech M, et al. Pancreatic stellate cells promote hapto-migration of cancer cells through collagen I-mediated signalling pathway. Br J Cancer 2014;110:409-20.
39. Teicher BA, Herman TS, Holden SA, et al. Tumor resistance to alkylating agents conferred by mechanisms operative only in vivo. Science 1990;247:1457-61.
40. Fujita H, Ohuchida K, Mizumoto K, et al. Tumor-stromal interactions with direct cell contacts enhance proliferation of human pancreatic carcinoma cells. Cancer Sci 2009;100:2309-17.

Figure Legends

Figure 1. Effect on cancer cells proliferation and apoptosis after combination treatment with Gemcitabine and ATRA.

Summary data from organotypic cultures (OT) and *LSL-Kras$^{G12D/+}$;LSL-Trp53$^{R172H/+}$;Pdx-1-Cre* mice (KPC mice) treated with either vehicle, Gemcitabine alone, ATRA alone or a combination of Gemcitabine with ATRA as shown by median and interquartile range as box and whisker (min-max) plots. All observations were normalized to controls (vehicle). 9-15 experimental replicates were carried out for OT resulting in 35-50 high power field measurements. 5-6 mice per group were enrolled to allow assessments in 10-30 high power fields. Comparisons were made by Kruskal-Wallis test followed by Dunn's post-hoc analysis. **** P<0.001, ** P< 0.01, * P<0.05*. PSC: Pancreatic stellate cell.

Cancer cell proliferation index in organotypics (A,B) and KPC mice (C).

Cancer cell apoptotic index in organotypics (D,E) and KPC mice (F).

Please see ~~**Supplementary Figure 2 for an example of method of calculation and**~~ Supplementary Figure **4**3 for representative images ~~**respectively**~~.

Figure 2. Effect on cancer and stellate cells invasion after combination treatment with Gemcitabine and ATRA.

Summary data from organotypic cultures (OT) and *LSL-Kras$^{G12D/+}$;LSL-Trp53$^{R172H/+}$;Pdx-1-Cre* mice (KPC mice) treated with either vehicle, Gemcitabine alone, ATRA alone or a combination of Gemcitabine with ATRA as shown by median and interquartile range as box and whisker (min-max) plots. All observations were normalized to controls (vehicle). 9-15 experimental replicates were carried out for OT resulting in 35-50 high power field measurements. 5-6 mice per group were enrolled to allow assessments in 10 high power fields. Comparisons were made by Kruskal-Wallis test followed by Dunn's post-hoc analysis. **** P<0.001*, *** P<0.01*, ** P<0.05*. PCC: Pancreatic cancer cell; PSC: Pancreatic stellate cell.

Cancer cell invasion index in organotypics (A,B).

Stellate cell invasion index in an organotypic model (C, D)

Stellate cell density in KPC mice (E). Stellate cell density in KPC was determined as green signal pixel intensity per area; the number of stellate cells was not counted as it was not possible to identify accurately this cell type in the KPC tumour section.

Please see Supplementary Figure ~~2 for an example of method of calculation and~~ 4 for representative images ~~respectively~~.

Figure 3. Effect on pancreatic stellate cell activity, vascularity and hypoxia after combination treatment with Gemcitabine and ATRA.

Summary data from organotypic cultures (OT) and *LSL-Kras$^{G12D/+}$;LSL-Trp53$^{R172H/+}$;Pdx-1-Cre* mice (KPC mice) treated with either vehicle, Gemcitabine alone, ATRA alone or a combination of Gemcitabine with ATRA as shown by median and interquartile range as box and whisker (min-max) plots. All observations were normalized to controls (vehicle). 9-15 experimental replicates were carried out for organotypics resulting in 35-50 high power field measurements. 5-6 mice per group were enrolled to allow assessments in 10-30 high power fields. Comparisons were made by Kruskal-Wallis test followed by Dunn's post-hoc analysis. **** P<0.001, ** P< 0.01, * P<0.05*. PSC: Pancreatic stellate cell.

Stellate cell activity in terms of fibronectin deposition in an organotypic model (A,B) and KPC mice (C) and, in terms of Collagen I deposition in the KPC mouse model (D).

Vascular density as determined by Endomucin stain in the KPC mouse model (E). Hypoxic index as determined by GLUT-1 stain (F).

Please see Supplementary Figures ~~2,~~ 5 and 6 ~~for method of calculation and~~ for representative images ~~respectively~~.

Figure 4. Effect of combination treatment with Gemcitabine and ATRA on tumour growth, Gemcitabine and ATRA intra-tumoural levels in KPC mice.

(A) Percentage necrotic area as determined by H&E slides. Summary data from *LSL-Kras$^{G12D/+}$;LSL-Trp53$^{R172H/+}$;Pdx-1-Cre* mice (KPC mice) treated with either vehicle, Gemcitabine alone, ATRA alone or a combination of Gemcitabine with ATRA as shown by median and inter-quartile range as box and whisker (min-max) plots. 5-6 mice per group were enrolled. Comparisons were made by Kruskal-Wallis test followed by Dunn's post-hoc analysis. **** P<.001, ** P< 0.01, * P<0.05*. See Supplementary Figure 6C for representative images.

(B) Percentage change in tumour volume between pre-treatment (Day -2) and post-treatment (Day 7) was measured by ultrasound in the KPC mouse model.

(C) Serum and pancreatic tumour ATRA concentration demonstrated correlation in mice receiving ATRA treatment (Pearson's correlation coefficient 0.66 (95% CI 0.09-0.9)). A regression line and it's 95% confidence intervals are shown.

(D) ATRA tumour tissue concentration in KPC mice treated with ATRA or Gem/ATRA

(E) Tumour Tissue Gemcitabine metabolites in Gem and Gem/ATRA treated mice.

~~**Please see Supplementary Figure 7 for methods of measurement.**~~

ns: not significant.

Figure 5: The combination of Gemcitabine with ATRA affects multiple embryonic signalling cascades in cancer cells and stroma in organotypic cultures and KPC mice.

Summary data from organotypic cultures (OT) and *LSL-Kras$^{G12D/+}$;LSL-Trp53$^{R172H/+}$;Pdx-1-Cre* mice (KPC mice) treated with either vehicle, Gemcitabine alone, ATRA alone or a combination of Gemcitabine with ATRA as shown by median and interquartile range as box and whisker (min-max) plots. All observations were normalized to controls (vehicle). Sections from three experimental replicates were carried out for organotypics resulting in 18

high power field measurements. Three mice per group were selected to allow assessments in 10 high power fields per section. Comparisons were made by Kruskal-Wallis test followed by Dunn's post-hoc analysis. *** *P<0.001, * P<0.05*.

FGF2 nuclear expression index in organotypics and KPC mice (A-C).

FGFR1 nuclear expression index in organotypics and KPC mice (D-F).

RARβ nuclear expression index in KPC mice (G).

sFRP4 stromal expression index in KPC mice (H).

Please see supplementary figures 7, 8 and 9 for representative images.

Figure 6: The combination of Gemcitabine with ATRA affects apical polarity, epithelial-mesenchymal transition and hedgehog signalling in cancer cells within organotypic cultures and KPC mice.

Representative images from organotypic cultures (OT) and *LSL-Kras$^{G12D/+}$;LSL-Trp53$^{R172H/+}$;Pdx-1-Cre* mice (KPC mice), as indicated, treated with either vehicle, Gemcitabine alone, ATRA alone or the combination of Gemcitabine with ATRA. Bold arrowheads used to indicate positive stain and other arrowheads to indicate negative stain.

A) Capan-1 cells stained with an anti-cytokeratin antibody (green) and anti-β-catenin (red) antibody was used to localize the presence of β-catenin in organotypic cultures. Cytokeratin positive cancer cells demonstrate loss of nuclear β-catenin in ATRA treated organotypic cultures. Please see Supplementary Figure 10 for detailed data on KPC mice and organotypic cultures. Scale bar 10μm.

B) Anti-cytokeratin antibody (green) and anti-Ezrin antibody (red) were used to localize the presence of Ezrin in KPC mice. Cytokeratin positive cancer cells demonstrate loss of membranous Ezrin in ATRA treated murine tissues. Please see Supplementary Figure 11 for detailed data on KPC mice and organotypic cultures.

C) Anti-cytokeratin antibody (green) and anti-Twist1 (red) antibody were used to localize the presence of *Twist1* in Capan1/PS1 organotypic cultures. Cytokeratin-positive cancer cells

demonstrate loss of nuclear *Twist1* in ATRA organotypic cultures. Cytokeratin negative PSC demonstrate nuclear *Twist1* to act as an internal positive control. Please see Supplementary Figure 12 for detailed data on KPC mice and organotypic cultures.

D) Anti-Zeb1 antibody (green) and anti-E-cadherin (red) antibody were used to localize the presence of *Zeb1* in Capan1/PS1 organotypic cultures. E-cadherin-positive cancer cells demonstrate loss of nuclear *Zeb1* in ATRA organotypic cultures. E-cadherin negative PSC demonstrate nuclear *Zeb1* to act as an internal positive control. Please see Supplementary Figure 13 for detailed data on KPC mice and organotypic cultures.

E) In KPC mice, anti-Gli1 staining (brown) was used to localize Gli1 expression. Loss of Nuclear Gli1 in epithelial appearing cells was demonstrable within ATRA treated murine PDAC tissues. Please see Supplementary Figure 14 for detailed data on KPC mice.

Scale bar 10μm.

Anti-stromal treatment together with chemotherapy targets multiple signalling pathways in pancreatic adenocarcinoma.

Elisabete F. Carapuça[1#], Emilios Gemenetzidis[1#], Christine Feig[2], Tashinga E. Bapiro[2], Michael D. Williams[2], Abigail S. Wilson[1], Francesca R. Delvecchio[1], Prabhu Arumugam[1], Richard P. Grose[1], Nicholas R Lemoine[3], Frances M. Richards[2], Hemant M Kocher[1,4]*

[1]Centres for Tumour Biology and [3]Molecular Oncology, Barts Cancer Institute – a CRUK Centre of Excellence, Queen Mary University of London, London EC1M 6BQ, UK.

[2]The University of Cambridge Cancer Research-UK Cambridge ~~Research~~ Institute, Li Ka Shing Centre, Robinson Way Cambridge, CB2 0RE, England.

[4]Barts and the London HPB Centre, The Royal London Hospital, Barts Health NHS Trust, London, E1 1BB, UK.

Running title: stroma and cancer co-targeting

***Corresponding author:** Hemant M Kocher MS MD FRCS, Queen Mary University of London, Centre for Tumour Biology, Barts Cancer Institute – a CRUK Centre of Excellence, Charterhouse Square, London EC1M 6BQ, UK.

Tel: +44(0) 20 7882 3579; Email: h.kocher@qmul.ac.uk

#Contributed equally

Supplementary Figure 1: Design of experiments and determination of dosing schedule.

A) Determination of Gemcitabine GI_{50} (Cytotoxic effect: growth inhibition of 50%) alone, or in combination with ATRA (1μM), on AsPC1 (blue and black lines) or Capan1 (green and red lines) cell growth. Pancreatic cancer cell lines AsPC-1 and Capan1 in 2D monoculture were exposed once, to different concentrations of Gemcitabine, and were allowed to grow for a period of up to seven days, prior to assessing proliferation rates. The GI_{50} for Gemcitabine was determined as 240nM for AsPC1, and 48nM for Capan1, indicating that AsPC1 cells are more resistant to Gemcitabine, when compared to Capan1 cell line. Addition of daily ATRA, to this treatment regimen had no effect on the GI_{50} curves of either cell line, indicating the lack of any combinational effect of ATRA with Gemcitabine in 2D monocultures on cancer cells.

B) Determination of Gemcitabine GI_{50} alone or in combination with ATRA (1μM) on pancreatic stellate cells (PSC) growth. PSC showed sensitivity to Gemcitabine (GI_{50} 26nM), which increased when treatment was combined with daily ATRA exposure. At least, in 2D cultures, the actively proliferating PSC appear to be sensitive to Gemcitabine.

C) i) Treatment protocol of the 3D organotypic cultures with Gemcitabine weekly for two consecutive weeks, mimicking treatment currently in use in the clinic (1). Representative images of H&E stained sections of gels resultant from AsPC1 **(ii)** or Capan1 **(iii)** organotypic cultures, treated with Gemcitabine at various doses in order to determine Gemcitabine GI_{50} (concentration that reduces epithelial cell layer thickness by 50%). Gemcitabine GI_{50} was slightly higher at 300nM for AsPC1 and 100nM for Capan1 organotypic cultures than in the 2D monocultures. The increased value of GI_{50} is anticipated due to cyto-protective effect of organized 3D matrix particularly Collagen I (2). Intriguingly PSC layer thickness was unaffected by Gemcitabine treatment, when PSC and cancer cells were combined (data not shown).

D) Representative image of a section of an organotypic culture treated with BrdU (red) and stained with a cytokeratin antibody (green) to delineate cancer cells. Representative graph of the percentage of cancer and stellate cells with BrdU incorporation. To determine the rates of nucleoside uptake in organotypic cultures, BrdU pulse chase was carried out. BrdU is an analogue of the nucleoside thymidine, and Gemcitabine an analogue of cytidine. BrdU was administered at the same concentrations that Gemcitabine would be added to the 3D co-culture models. The percentage of incorporation of BrdU by PSC was much less than by tumour cells, which confirms that Gemcitabine has minimal cytotoxic effect on PSC in organotypic culture model. This effect may be due to a slower proliferation rate of PSC. Thus, they do not incorporate the nucleoside analogue at the same rate as cancer cells. Therefore, the cytotoxic effect of Gemcitabine is largely specific to the epithelial cancer cells.

~~**D)** Design of organotypic treatment regimen: **i)** Previously, in order to dissect this cell-specific targeting, organotypic cultures were treated with ATRA (1μM) for a period of 10 days (3). However, this model/schedule lacked features of advanced pancreatic cancer (4). **ii)** Hence, we allowed epithelial-stellate cell interaction to be established for ten days before commencing treatment. Organotypic cultures were treated with either Gemcitabine once weekly, mimicking the regimen treatment being currently being given to patients in the clinic(1), or ATRA daily, again using a clinically relevant protocol (5), or with the combination of both or their respective vehicles.~~

~~**E)** KPC mice treatment scheme: Compound mutant KPC mice with mature, established tumours were enrolled at a median age of 180 days and used as described previously (3, 6). Mice were treated with Gemcitabine at 100 mg/Kg by intraperitoneal injection on a Q3Dx4 schedule, and with ATRA daily at 15 mg/Kg by oral gavage, or the combination of both at the appropriate times. The volume of the tumours was measured by ultrasound two days before the beginning of the treatment, and mice bearing tumour volume of an average 250 mm^3 were selected for the study. .~~

Supplementary Figure 2: Determination of marker expression fold-change.

A) i) Representative image of a Photoshop screen shot of an organotypic section, stained with a anti-cytokeratin antibody (green) to identify cancer cells and with an anti-Fibronectin (FN) antibody (red) to identify FN expression by PSC. The window tool selects the colour range of the marker (FN) under study.

ii) Pre-specified colour range attributes were loaded from one common .AXT colour range file to ensure equal pixel detection across samples (shown now in a black & white channel). This would assess the pixel number that will represent the marker expression intensity, in this case FN.

iii) Representative histogram indicating the pixel number detected accordingly with the colour range selected.

B) i) Graphic representation of the number of pixels from FN expression per field of a gel, in a total of three gels for one biological repeat, across all treatment conditions. At least four images per gel were analysed for the quantification of fibronectin.

ii) Graphic representation of the median number of pixels from FN expression as summarized per gel.

C) i) Representative image of an Image J screenshot of the same organotypic section as in Ai), and of the window tool used to quantify the stellate cell number based on the nuclei morphology, size and absence of cytokeratin stain.

ii) Representative graph of FN pixel number normalized to total PSC number (FN index) per gel, in a total of three gels from one biological experiment, for each arm of treatment.

D) Graphic representation of FN index from three biological experiments, as shown in (Bii) for one single biological experiment. This summary graph would represent one graph in the Main Figure for each attribute investigated.

Supplementary Figure 2: The combination treatment of Gemcitabine with ATRA does not affect PSC number, and consequently gel length and thickness is also unchanged.

A) Schematic representation of an organotypic culture of admixed cancer cells and PSC, seeded on top of gel composed of Matrigel and Collagen I that mimics the tumour ECM environment. Measurements of cancer cell layer thickness, gel length, gel thickness are schematically represented and have been previously described (3).

B, C) Cancer cell layer thickness was unaffected in presence of PSC in Capan1/PS1 (B) and AsPC1/PS1 (C) organotypic cultures, respectively, upon treatment with vehicle, Gemcitabine alone, ATRA alone or a combination of Gemcitabine and ATRA.

D,E) Total PSC number was also unaffected in Capan1/PS1 (D) and AsPC1/PS1 (E) organotypic cultures respectively upon treatment.

F,G) Gel thickness was also unaffected in Capan1/PS1 (F) and AsPC1/PS1 (G) organotypic cultures, respectively, upon treatment.

H,I) Gel length was also unaffected in Capan1/PS1 (H) and AsPC1/PS1 (I) organotypic cultures, respectively, upon treatment.

9-15 experimental replicates were carried out for organotypic cultures. Comparisons were made by Kruskal-Wallis test followed by Dunn's post-hoc analysis.

ns: not significant

Supplementary Figure 3: The combination of Gemcitabine with ATRA affects cancer cell proliferation, apoptosis ~~and invasion~~ in organotypic cultures, as well as ~~cancer cell proliferation and apoptosis~~ in KPC mice.

A) Representative images from organotypic cultures (OT) treated with either vehicle, Gemcitabine alone, ATRA alone or the combination of Gemcitabine with ATRA. Capan1 cells stained with an anti-cytokeratin antibody (green) and proliferating Capan1 cells stained with an anti-Ki67 antibody (red) to determine ratio of proliferating cancer cells per field.

B) Representative images of tumour sections from *LSL-Kras$^{G12D/+}$;LSL-Trp53$^{R172H/+}$;Pdx-1-Cre* mice (KPC mice) treated with vehicle, Gemcitabine, ATRA or Gemcitabine with ATRA, and stained with an anti-CK8 antibody (red) and proliferating cancer cells stained with an anti-Ki67 antibody (green) to determine the ratio of proliferating cancer cells per field.

C) Representative images from organotypic cultures (OT) after same treatment regimen, where Stellate cells were stained with an anti-alpha-SMA antibody in green and with an anti-Ki67 antibody (red) to determine ratio of proliferating stellate cells per field.

D) Representative images of organotypic gel sections where Capan1 cells were stained by immuno-histochemistry with an anti-cleaved caspase-3 antibody. Apoptotic cancer cells were identified by the cytoplasmic brown staining. There was no staining within the PSC layer. Percentage apoptotic cancer cells (based on morphology) were determined.

E) Representative images of tumour sections from KPC mice stained with an anti-cleaved caspase-3 antibody to determine apoptotic cells. There was no staining in non-epithelial compartment. Percentage apoptotic cancer cells (based on morphology) were determined.

F) Representative images of tumour sections from KPC mice stained by immunofluorescence with an anti-alpha-SMA antibody and with an anti-cleaved caspase-3 antibody to determine the ratio of apoptotic stellate cells. There was no staining in the stromal compartment.

Supplementary Figure 4: The combination of Gemcitabine with ATRA affects cancer and stellate cell invasion in organotypic cultures as well as stellate cells density in KPC mice.

A) Representative images of organotypic gel sections where Capan1 cells were stained with a cytokeratin antibody (green) and PSC were stained with an anti-αSMA antibody (red) to identify the cells that have invaded the gel. The yellow line marks the junction between the PSC layer and the extracellular matrix (top of the gel). The number of invading cells was counted directly on the section on the Axioplan microscope, to accurately identify the top of the gel and identify the cell type and number that invaded into the gel.

B) i and ii) Representative H&E stained image from a Capan-1/PS1 OT section that clearly shows the cancer cell layer, the gel and the top of the gel where the stellate cell layer is demonstrable. The dashed black line in ii) marks the top of the gel. Invading cells were counted below the black line..

C) Representative images of tumour sections from KPC mice stained with an anti-αSMA antibody (green) to identify PSC. Stromal cell density was determined by green pixel intensity. Pericytes were accounted for as described in Figure 6A. Scale bar 100 μm (except C where Scale bar = 50 μm).

Supplementary Figure 5: ATRA alters stellate cells activation status.

A) Representative images of organotypic sections where Capan1 cells were stained with an anti-Cytokeratin antibody (green) and extra-cellular matrix (ECM) deposition by an anti-Fibronectin antibody (red). Note: the ECM gel formed at inception with Collagen I and Matrigel contains no fibronectin. Hence, fibronectin shown here represents ECM generated by cells co-cultured in 3D. Fibronectin deposition was only present around PSC, indicating PSC were source of this ECM protein. Fibronectin deposition was normalized to PSC number to determine PSC activity as shown in Supplementary Figure 2. Scale bar 100 µm.

B) Representative images of tumour sections from *LSL-Kras$^{G12D/+}$;LSL-Trp53$^{R172H/+}$;Pdx-1-Cre* mice (KPC mice) stained by immuno-histochemistry with anti-Fibronectin antibody. Fibronectin expression was scored based on intensity and degree of brown staining as described before (4). Scale bar 50 µm.

C) Representative images of Collagen deposition in KPC mice tumour sections stained with Picrosirius Red. Pixel intensity was determined as described before (5). Scale bar 100 µm.

Supplementary Figure 6: The combination treatment of Gemcitabine with ATRA alters the vascular density, hypoxic environment and the necrosis pattern in murine tumours.

A) Representative images of tumour sections from *LSL-Kras$^{G12D/+}$;LSL-Trp53$^{R172H/+}$;Pdx-1-Cre* mice (KPC mice) stained with an anti-Endomucin antibody (red) to identify blood vessels and an anti-αSMA antibody (green) to identify stellate cells as well as pericytes. The number of blood vessels increased in the tumour/stromal area of PDAC tumours of mice treated with ATRA or with the combination Gemcitabine /ATRA, while at the same time there is a reduction of αSMA expression (after subtracting doubly stained structures to exclude pericytes). Scale bar 100 μm.

B) Representative images KPC mice tumour sections stained with an anti-GLUT1 antibody (green) to mark hypoxic areas in the tumours. Pixel intensity determined level of hypoxia as described before (6). Scale bar 100 μm.

C) Representative images of H&E stained tumour sections from mice. Necrotic areas, identified by morphology, are marked by the dotted lines in black. Percentage of necrotic area was determined based on total surface area of tumour. Scale bar 5000 μm.

~~**Supplementary Figure 7: Determination of murine tumour volume and tumour and serum concentration of ATRA and Gemcitabine with its metabolites.**~~

~~**A)** Representative image of ultrasound measurements and formula used to determine tumour volume at various time points.~~

~~**B)** Enrolment volume of the murine tumours. There is no significant difference of volume amongst the tumours. Comparisons were made by Kruskal-Wallis test followed by Dunn's post-hoc analysis.~~

~~**C)** Chromatogram system suitability test for ability to separate ATRA from 9-cis and 13-cis isomers of retinoic acid.~~

~~**D)** Chromatogram of Plasma Extract from Mouse 8362.~~

Supplementary Figure 7: ATRA treatment affects pancreatic stellate cell activity by reducing the nuclear translocation FGF2.

A-D) Representative images of sections from *LSL-Kras$^{G12D/+}$;LSL-Trp53$^{R172H/+}$;Pdx-1-Cre* mice (KPC mice) stained with an anti-FGF2 antibody (red) and an anti-Cytokeratin antibody (green) to identify epithelial cells.

E-H) Representative images of Capan1/PS1 organotypic (OT) sections stained with same antibodies as KPC mice. There is a clear reduction of nuclear FGF2 expression in stromal cells (Cytokeratin –ve cells) from mice treated with ATRA. Scale bar 50 μm.

a-d) Zoom in images of the marked areas of KPC main images (A-D) with bold arrowheads pointing to nuclear FGF2 expressing stromal cells and empty arrowheads pointing to stromal cells not expressing FGF2 in the nucleus.

e-h) Zoom in images of the marked areas of OT main images (E-H) also with bold and empty arrowheads pointing to the difference of nuclear FGF2 expression in stellate cells upon treatment with ATRA. Scale bar 10 μm.

Supplementary Figure 8: ATRA treatment affects the pancreatic stellate cell activity by reducing the nuclear translocation of FGFR1.

A-D) Representative images of sections from *LSL-Kras$^{G12D/+}$;LSL-Trp53$^{R172H/+}$;Pdx-1-Cre* mice (KPC mice) stained with an anti-FGFR1 antibody (red) and an anti-αSMA antibody (green) to identify stromal cells.

E-H) Representative images of Capan1/PS1 organotypic (OT) sections stained with same antibodies as KPC mice. There is a clear reduction of nuclear FGFR1 expression in stromal αSMA-positive cells in the mice treated with ATRA. Scale bar 50 μm.

a-d) Zoom in images of the marked areas of KPC main images (A-D) with bold arrowheads pointing to nuclear FGFR1 expressing stromal cells and empty arrowheads pointing to stromal cells with no nuclear FGFR1 expression.

e-h) Zoom in images of the marked areas of OT main images (E-H) also with bold and empty arrowheads pointing to the difference of nuclear FGFR1 expression in stellate cells upon treatment with ATRA which is in concordance with FGF2 expression pattern seen in Supplementary figure 8. Scale bar 10 μm.

Supplementary Figure 9: Nuclear RARβ expression in, and stromal sFRP4 secretion by, pancreatic stellate cells is altered upon treatment with ATRA alone and in combination with Gemcitabine.

A) Representative images of tumour sections from *LSL-Kras$^{G12D/+}$;LSL-Trp53$^{R172H/+}$;Pdx-1-Cre* mice (KPC mice) stained by immuno-histochemistry with an anti-RARβ antibody. Nuclear RARβ expression is most enhanced in stellate cells of sections from mice treated with ATRA. Zoom in images show the amplification of the marked areas of main images, which show the nuclear RARβ expression in stetalle cells of sections from ATRA treated mice in comparison to Vehicle or Gemcitabine alone treated mice. Scale bar 100 μm. Zoom in images: Scale bar 10 μm.

B) Representative images of tumour sections from KPC mice stained by immuno-histochemistry with an anti-sFRP4 antibody. Stromal sFRP4 expression is most enhanced in tumour surrounding environment of sections from mice treated with ATRA alone or in combination with Gemcitabine. Scale bar 50 μm. Zoom in images show a significant expression of sFRP4 in the stroma of tumour from ATRA or ATRA/Gemcitabine combination treated mice in comparison to Vehicle or Gemcitabine alone treated mice. Zoom in images: Scale bar 10 μm.

Supplementary Figure 10: ATRA disrupts Wnt-β-catenin signalling pathway.

A-D) Representative images of tumour sections from *LSL-Kras$^{G12D/+}$;LSL-Trp53$^{R172H/+}$;Pdx-1-Cre* mice (KPC mice) stained with an anti-β-catenin antibody (red) and an anti-Cytokeratin antibody (green) to identify epithelial cells.

E-H) Representative images of Capan1/PS1 organotypic (OT) sections stained with same antibodies as KPC mice sections. Scale bar 50 μm.

a-d) Zoom in images of the marked areas of KPC main images (A-D) with bold arrowheads pointing to nuclear β-catenin expression in epithelial cells and empty arrowheads pointing to no nuclear β-catenin expression.

e-h) Zoom in images of marked areas of OT main images (E-H) also with bold and empty arrowheads pointing to the differences of nuclear β-catenin expression in epithelial cells. There is a shift of the spatial β-catenin localization that spans from the cell nuclei, in epithelial cell either from KPC tumours or OT cultures treated with vehicle or Gemcitabine alone to the cell membrane upon treatment with ATRA or Gemcitabine and ATRA. Scale bar 10 μm.

Supplementary Figure 11: The combination treatment affects the lumen formation and apico-basal polarity of cancer cells.

A-D) Representative images of tumour sections from *LSL-Kras$^{G12D/+}$;LSL-Trp53$^{R172H/+}$;Pdx-1-Cre* mice (KPC mice) stained with an anti-Ezrin antibody (red) and an anti-Cytokeratin antibody (green) to identify epithelial cells.

E-H) Representative images of Capan1/PS1 organotypic (OT) sections stained with same antibodies as KPC mice sections. Scale bar 50 µm.

a-d) Zoom in images of the marked areas of KPC main images (A-D) with bold arrowheads pointing to Ezrin cell membrane expression in cancer cells and empty arrowheads pointing to loss of membranous Ezrin expression.

e-h) Zoom in images of the marked areas of OT main images (E-H) also with bold and empty arrowheads pointing to the differences in Ezrin expression in cancer cells. Ezrin expression is reduced in cancer cells of KPC mice tumours or OT cultures, after the combination treatment (Gemcitabine with ATRA). Scale bar 10 µm.

Supplementary Figure 12: ATRA alone or in combination with Gemcitabine nuclear *Twist*1 expression within cancer cells.

A-D) Representative images of tumour sections from *LSL-Kras*$^{G12D/+}$;*LSL-Trp53*$^{R172H/+}$;*Pdx-1-Cre* mice (KPC mice) stained with an anti-Twist1 antibody (red) and an anti-Cytokeratin antibody (green).

E-H) Representative images of Capan1/PS1 organotypic (OT) sections stained with same antibodies as KPC mice sections. Scale bar 50 μm.

a-d) Zoom in images of the marked areas of KPC main images (A-D) with bold arrowheads pointing to nuclear *Twist*1 expression in epithelial cells expression and empty arrowheads pointing to loss of this nuclear *Twist*1 expression.

e-h) Zoom in images of the marked areas of OT main images (E-H) also with bold and empty arrowheads pointing to the differences of nuclear *Twist*1 expression in epithelial cells upon different treatment conditions. ATRA alone or in combination with Gemcitabine reduces nuclear *Twist*1 expression in epithelial cells, whilst in stellate cells nuclear *Twist*1 expression remains unaltered. Scale bar 10 μm.

Supplementary Figure 13: The combination treatment affects the nuclear translocation of transcription factor *ZEB*1 in cancer cells.

A-D) Representative images of tumour sections from *LSL-Kras*$^{G12D/+}$*;LSL-Trp53*$^{R172H/+}$*;Pdx-1-Cre* mice (KPC mice) stained with an anti-Zeb1 antibody (red) and an anti-αSMA antibody (green).

E-H) Representative images of Capan1/PS1 organotypic (OT) sections stained with an anti-E-cadherin antibody (red) and an anti-Zeb1 antibody (green). Scale bar 50 μm.

a-d) Zoom in images of the marked areas of KPC main images (A-D) with bold arrowheads pointing to nuclear *Zeb1* expression within epithelial cells and empty arrowheads pointing to loss of nuclear *Zeb*1 expression.

e-h) Zoom in images of the marked areas of OT main images (E-H) also with bold and empty arrowheads pointing to the differences of nuclear *Zeb*1 expression in epithelial cells upon different treatment conditions. ATRA in combination with Gemcitabine reduces nuclear *Zeb*1 expression in epithelial cells, whilst in stellate cells nuclear *Zeb*1 expression remains unaltered. Scale bar 10 μm.

Supplementary Figure 14: The combination treatment affects the Hedgehog signalling in cancer cells.

A) Representative images of tumour sections from *LSL-Kras$^{G12D/+}$;LSL-Trp53$^{R172H/+}$;Pdx-1-Cre* mice (KPC mice) stained by immuno-histochemistry with an anti-Gli1 antibody. Zoom in images show the clear expression of nuclear and cytoplasmic Gli1 in ductal cells sections from untreated or Gemcitabine treated mice in comparison to a reduction of Gli1 expression in cancer cells of ATRA/Gemcitabine treated mice.

B) Representative images of OT sections stained by immuno-histochemistry with an anti-Gli1 antibody. Zoom in images clearly show the reduction in Gli expression of cancer cells from Gemcitabine/ATRA treated OT cultures, which is in agreement with the differences in Gli1 expression also observed in KPC mice. Scale bar 100 μm. Zoom in images: Scale bar 10 μm.

Supplementary table 1: KPC mice characteristics at recruitment

Treatment type	Age (days)	Tumour volume (mm^3 on 2 days before treatment as measured by ultrasound)
Control	249	137.761
Control	188	303.706
Control	170	326.367
Control	117	163.306
Control	120	195.04
Control	128	149.467
Gemcitabine	211	124.714
Gemcitabine	200	274.747
Gemcitabine	189	232.725
Gemcitabine	177	284.779
Gemcitabine	176	149.722
Gemcitabine	102	191.824
ATRA	216	156.138
ATRA	177	302.217
ATRA	243	327.712
ATRA	223	211.803
ATRA	150	160.042
ATRA + Gemcitabine	119	324.267
ATRA + Gemcitabine	171	234.933
ATRA + Gemcitabine	185	263.636
ATRA + Gemcitabine	218	495.181
ATRA + Gemcitabine	204	239.703
ATRA + Gemcitabine	124	343.271

Supplementary table 2: Table of antibodies

Sections species origin	Antibody	Catalogue reference	Incubation period	Antigen retrieval method	IF (or IHC) dilution
Organotypic sections (anti-human)	Rabbit Cytokeratin	DAKO Z0662	1h, RT	HIER	1:200
	Mouse Fibronectin	SIGMA F0916	ON, 4^0C	Pepsin	1:100
	Mouse Ki67	DAKO M7240	1h, RT	HIER	1:100
	Mouse αSMA	DAKO M0851	1h, RT	HIER	1:300
	Rabbit CC3	Cell signaling D175	1h, RT	HIER	1:400 (IHC)
	Rabbit Gli1*	Chemicon AB3444	1h, RT	HIER	1:300 (IHC)
	Mouse E-Cadherin	Abcam ab1416	ON, 4^0C	HIER	1:100
	Rabbit RAR-β*	Abcam ab53161	1h, RT	HIER	1:200 (IHC)
	Mouse Twist1*	Abcam ab50887	ON, 4^0C	HIER	1:100
	Rabbit Zeb1*	Santa cruz sc-25388	ON, 4^0C	HIER	1:500
	Mouse FGF2*	Millipore 05-118	ON, 4^0C	HIER	1:100
	Rabbit FGFR1*	Abcam ab10646	ON, 4^0C	HIER	1:500
	Rabbit SFRP4*	Santa cruz sc-30152	1h, RT	N.A.	1:50 (IHC)
	Mouse Ezrin*	BD 10603	ON, 4^0C	HIER	1:200
	Mouse β-Catenin*	BD 610154	ON, 4^0C	HIER	1:200
KPC mouse sections (anti-mouse)	Rabbit CK8	Abcam ab59400	ON, 4^0C or 1h, RT	HIER	1:100
	Rabbit Fibronectin	Abcam ab23750	1h, RT	HIER	1:200 (IHC)
	Rabbit Ki67	Abcam ab15580	1h, RT	HIER	1:150
	Mouse αSMA	SIGMA F3777	ON, 4^0C	HIER	1:500
	Rabbit CC3	Cell signaling	1h, RT	HIER	1:400 (IHC)

		D175			
	Rat Endomucin	Santa Cruz Sc-65495	1h, RT	HIER	1:100
	Rabbit Glut1	Millipore 07-1401	ON, 4^0C	HIER	1:250

ON: overnight; 1h: one hour, RT; room temperature;

HIER: Heat Induced Epitope Retrieval (citrate buffer pH6)

N.A.: not applicable

*: used also in mouse

References:

1. The use of gemcitabine for the treatment of pancreatic cancer (TA25). In: National Institute for Health and Clinical Excellence; 2001.
2. Dangi-Garimella S, Sahai V, Ebine K, Kumar K, Munshi HG. Three-dimensional collagen I promotes gemcitabine resistance in vitro in pancreatic cancer cells through HMGA2-dependent histone acetyltransferase expression. PLoS One 2013;8:e64566.
3. Kadaba R, Birke H, Wang J, Hooper S, Andl CD, Di Maggio F, Soylu E, et al. Imbalance of desmoplastic stromal cell numbers drives aggressive cancer processes. J Pathol 2013;230:107-117.
4. Ene-Obong A, Clear AJ, Watt J, Wang J, Fatah R, Riches JC, Marshall JF, et al. Activated pancreatic stellate cells sequester CD8+ T cells to reduce their infiltration of the juxtatumoral compartment of pancreatic ductal adenocarcinoma. Gastroenterology 2013;145:1121-1132.
5. Wong P-P, Demircioglu F, Ghazaly E, Alrawashdeh W, Stratford MR, Scudamore CL, Cereser B, et al. Dual-action combination therapy enhances angiogenesis while reducing tumor growth and spread. Cancer Cell 2015:In Press.
6. Wong PP, Demircioglu F, Ghazaly E, Alrawashdeh W, Stratford MR, Scudamore CL, Cereser B, et al. Dual-action combination therapy enhances angiogenesis while reducing tumor growth and spread. Cancer Cell 2015;27:123-137.

PS1 proliferation assessed by Ki67 staining of AsPC1/PS1 OT sections

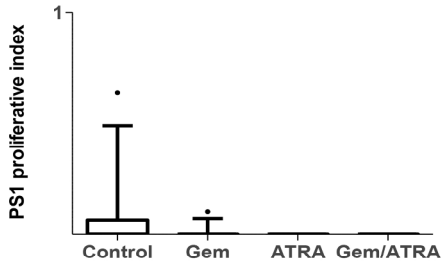

Results from the quantification of three technical replicates from one biological repeat of AsPC1/PS1 OT culture.

Table Analyzed	AsPC1/PS1 PS1 proliferation/HPF
Kruskal-Wallis test	
P value	0.0903
Exact or approximate P value?	Gaussian Approximation
P value summary	ns
Do the medians vary signif. (P < 0.05)	No
Number of groups	4
Kruskal-Wallis statistic	6.484

Dunn's Multiple Comparison Test	Difference in rank sum	Significant? P < 0.05?	Summary
Control vs Gem	4.083	No	ns
Control vs ATRA	6.042	No	ns
Control vs Gem/ATRA	6.042	No	ns
Gem vs ATRA	1.958	No	ns
Gem vs Gem/ATRA	1.958	No	ns
ATRA vs Gem/ATRA	0.0	No	ns

190x254mm (300 x 300 DPI)

Gem_ATRA paper

Staining for vessel:

- Performed lots of tests for CD31 Ab (**BD Pharmingen purified Rat Anti-Mouse CD31, cat. 550274**):
  - CD31 1:100 o/n incubation, cytrate buffer microwave, vectastain kit
  - CD31 1:70 o/n incubation, cytrate buffer microwave, vectastain kit
  - **CD31 1:70, 1hr, protease digestion at 37 C**
  - CD31 1:50, 1hr, pressure cooker and antigen unmasking solution from Foggy,
  - CD31 1:100, pronase 500 ug/ml, with saturation step
  - CD31 1:100, pronase 500 ug/ml, without saturation step
  - CD31 1:100, pronase 1:3, with saturation step
  - CD31 1:100, pronase 1:3, without saturation step
  - CD31, PROTEASE RTU from George, RT, on embryo
  - CD31 1:100, cytrate buffer and pressure cooker
  - CD31 1:200
  - CD31 1:400
  - CD31 1:100, pronase 1 mg/ml
  - CD31 1:200
  - CD31 1:400
  - CD31 1:100, pronase 10 mg/ml
  - CD31 1:200
  - CD31 1:400

240x187mm (300 x 300 DPI)

CD31 tested on kidney

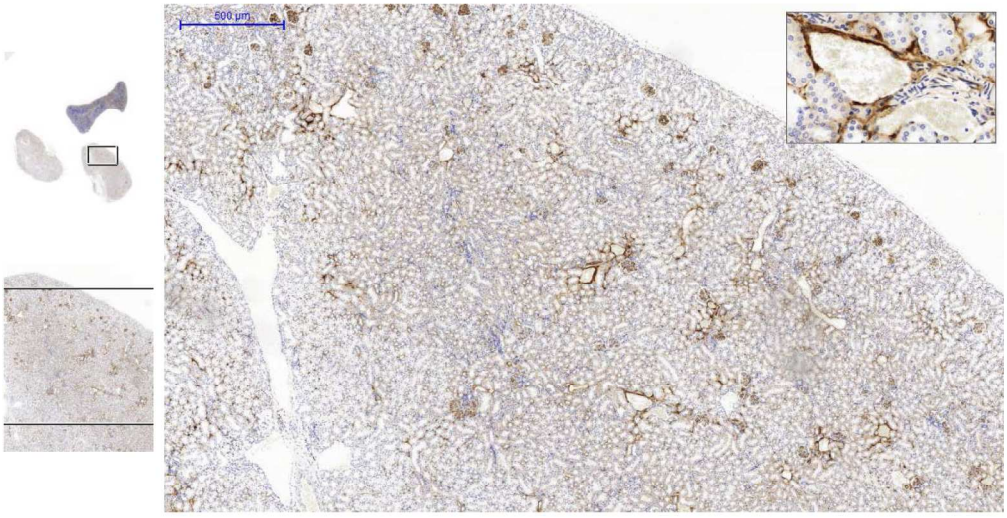

CD31 1:70, pronase 15', 37 degrees worked fine. Isotype control not good

252x176mm (300 x 300 DPI)

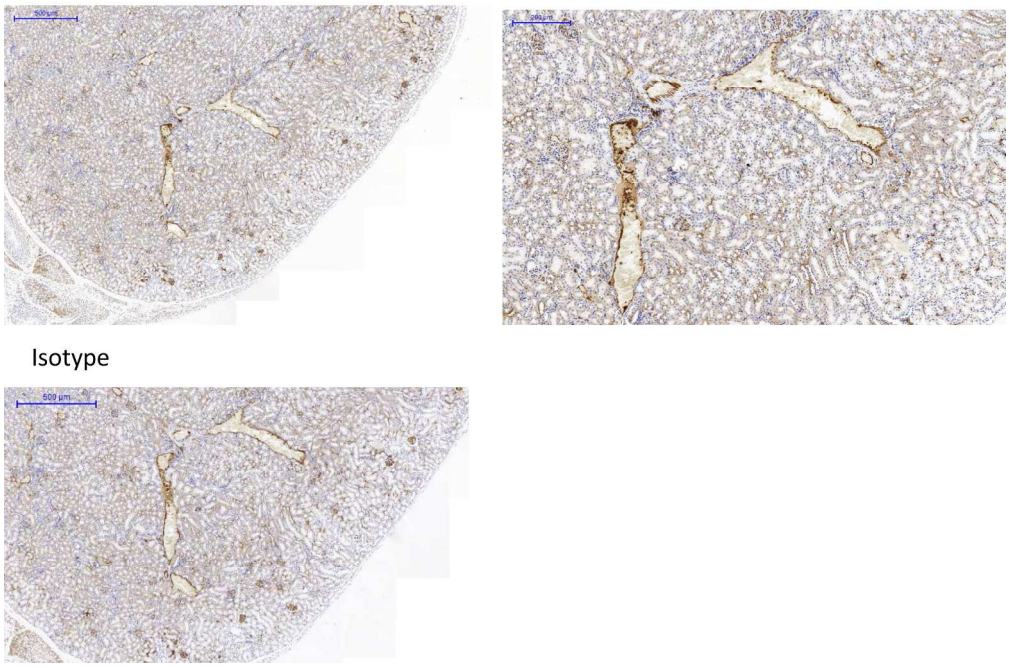

245x187mm (300 x 300 DPI)

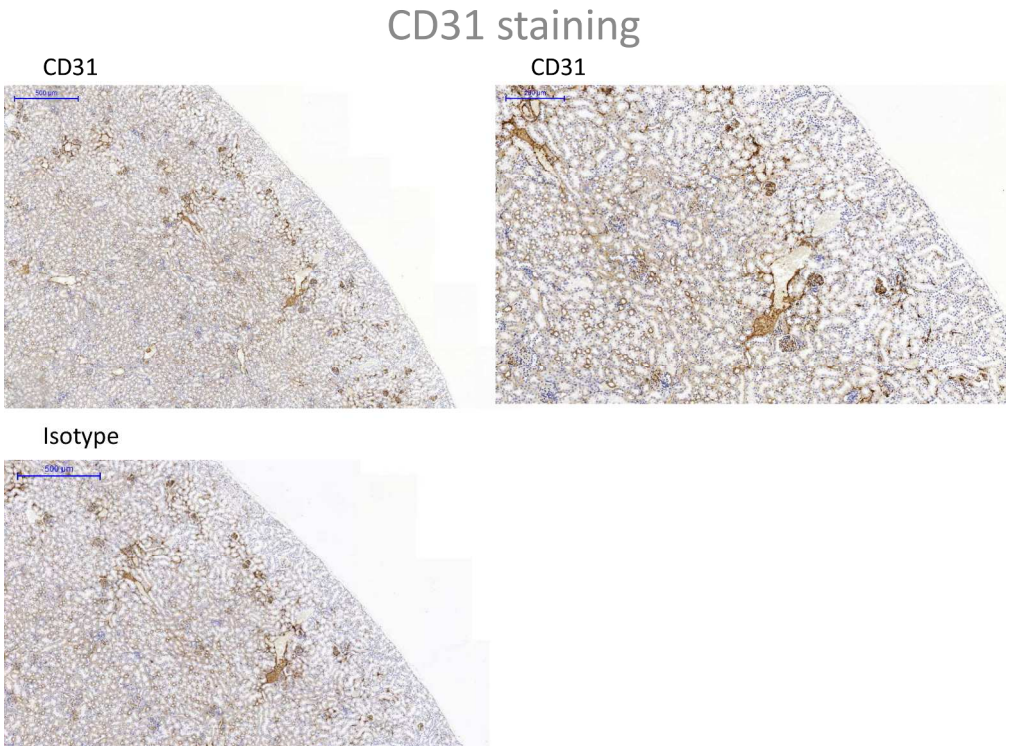

247x187mm (300 x 300 DPI)

Endomucin

Endomucin

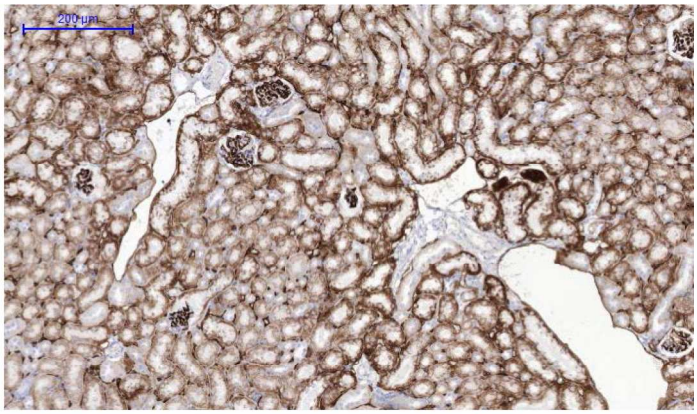

Isotype

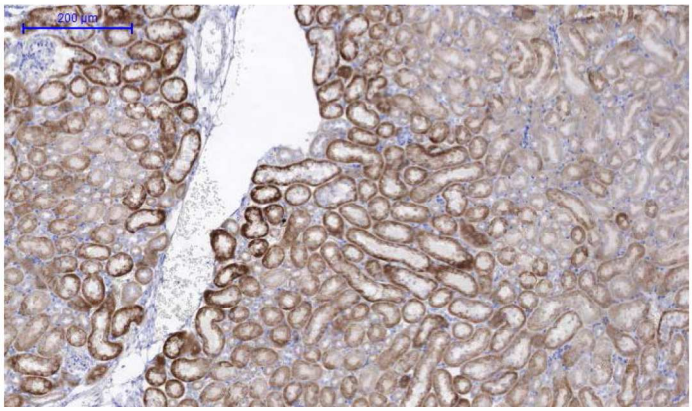

187x187mm (300 x 300 DPI)

Table Analyzed	AsPC1/PS1 PS1 norm activation/gel		
Kruskal-Wallis test			
P value	0.0006		
Exact or approximate P value?	Gaussian Approximation		
P value summary	***		
Do the medians vary signif. (P < 0.05)	Yes		
Number of groups	4		
Kruskal-Wallis statistic	17.19		
		Significant? P <	
Dunn's Multiple Comparison Test	Difference in rank sum	0.05?	Summary
Control vs Gem	9.931	No	ns
Control vs ATRA	14.26	Yes	*
Control vs Gem/ATRA	20.04	Yes	***
Gem vs ATRA	4.333	No	ns
Gem vs Gem/ATRA	10.11	No	ns
ATRA vs Gem/ATRA	5.778	No	ns

232x102mm (300 x 300 DPI)

Number of values	8	9	9	9
Minimum	0.3788	0.2451	0.1277	0.0
25% Percentile	0.8787	0.3754	0.2281	0.04974
Median	1.000	0.4655	0.3679	0.1330
75% Percentile	1.167	0.5239	0.4855	0.3205
Maximum	1.202	0.6201	0.6925	1.023
Mean	0.9553	0.4530	0.3711	0.2406
Std. Deviation	0.2641	0.1116	0.1761	0.3227
Std. Error	0.09336	0.03719	0.05870	0.1076
Lower 95% CI of mean	0.7346	0.3673	0.2357	-0.007467
Upper 95% CI of mean	1.176	0.5388	0.5065	0.4887
KS normality test				
KS distance	0.2603	0.1978	0.1296	0.3473
P value	> 0.10	> 0.10	> 0.10	0.0025
Passed normality test (alpha=0.05)?	Yes	Yes	Yes	No
P value summary	ns	ns	ns	**
Shapiro-Wilk normality test				
W	0.8308	0.9487	0.9645	0.7191
P value	0.0605	0.6753	0.8443	0.0024
Passed normality test (alpha=0.05)?	Yes	Yes	Yes	No
P value summary	ns	ns	ns	**
Sum	7.643	4.077	3.340	2.165

157x161mm (300 x 300 DPI)